

Multi-Node Wireless Energy Charging in Sensor Networks

Liguang Xie, *Member, IEEE*, Yi Shi, *Senior Member, IEEE*, Y. Thomas Hou, *Fellow, IEEE*, Wenjing Lou, *Senior Member, IEEE*, Hanif D. Sherali, and Scott F. Midkiff, *Senior Member, IEEE*

Abstract—Wireless energy transfer based on magnetic resonant coupling is a promising technology to replenish energy to a wireless sensor network (WSN). However, charging sensor nodes one at a time poses a serious scalability problem. Recent advances in magnetic resonant coupling show that multiple nodes can be charged at the same time. In this paper, we exploit this multi-node wireless energy transfer technology and investigate whether it is a scalable technology to address energy issues in a WSN. We consider a wireless charging vehicle (WCV) periodically traveling inside a WSN and charging sensor nodes wirelessly. Based on charging range of the WCV, we propose a cellular structure that partitions the two-dimensional plane into adjacent hexagonal cells. We pursue a formal optimization framework by jointly optimizing traveling path, flow routing, and charging time. By employing discretization and a novel *Reformulation-Linearization Technique* (RLT), we develop a provably near-optimal solution for any desired level of accuracy. Through numerical results, we demonstrate that our solution can indeed address the charging scalability problem in a WSN.

Index Terms—Optimization, scalability, wireless energy transfer, wireless sensor network.

I. INTRODUCTION

WIRELESS energy transfer based on magnetic resonant coupling is widely regarded as a breakthrough technology in our time [12]. By having magnetic resonant coils operating at the same resonant frequency, Kurs *et al.* demonstrated that energy could be transferred efficiently from a source coil to a receiver coil via nonradiative electromagnetic field (without any physical contact, i.e., wirelessly).¹ What makes such wireless energy transfer technology particularly attractive is that it is efficient even under omnidirection, does not require line-of-sight (LOS), and is insensitive to the neighboring environment. Since its inception, magnetic resonant coupling has

Manuscript received August 01, 2012; revised April 10, 2013 and October 05, 2013; accepted January 02, 2014; approved by IEEE/ACM TRANSACTIONS ON NETWORKING Editor S. Sen. This work was supported in part by the NSF under Grants 0925719, 1064953, 1156311, and 1156318 and the ONR under Grant N000141310080. An abridged version of this paper appeared in the IEEE Communications Society Conference on Sensor, Mesh and Ad Hoc Communications and Networks (SECON), Seoul, Korea, June 18–21, 2012.

The authors are with Virginia Tech, Blacksburg, VA 24061 USA (e-mail: xie@vt.edu; yshi@vt.edu; thou@vt.edu; wjlou@vt.edu; hanifs@vt.edu; midkiff@vt.edu).

Color versions of one or more of the figures in this paper are available online at <http://ieeexplore.ieee.org>.

Digital Object Identifier 10.1109/TNET.2014.2303979

¹It is important to note that magnetic resonant coupling is different from another technology called radiative energy transfer [17], [19]. The latter has much lower energy transfer efficiency. See Section II for more details.

quickly found commercial applications (see, e.g., [15], [18], and [26]).

In [25], we first applied this technology to a wireless sensor network (WSN) and showed that through periodic wireless energy transfer, a WSN could remain operational forever, i.e., infinite lifetime. Specifically, we showed that by having a wireless charging vehicle (WCV) visit each sensor node in the network and charge it periodically, one can ensure that each sensor node never runs out of energy.

An open problem in [25] is scalability of wireless charging. That is, as the node density increases in a WSN, how can a WCV ensure that each node is charged in a timely manner before it runs out of energy? The wireless charging technology developed in [12] was limited to charging one node at a time and is not scalable as node density increases.

Kurs *et al.* also recognized this problem and recently developed an enhanced technology (by properly tuning coupled resonators) that allows energy to be transferred to *multiple* receiving nodes simultaneously [13]. Interestingly, they showed that the overall efficiency was larger when charging multiple devices than charging each device individually.

Inspired by this new advance in wireless energy transfer, in this paper, we explore how such multi-node charging technology can address the scalability problem in charging a WSN. Following the setting in [25], we consider a WCV periodically traveling inside the network and charging sensor nodes. Upon completing each trip, the WCV returns to its home service station, takes a “vacation,” and starts out for its next trip. In contrast to [25], the WCV is now capable of charging multiple nodes at the same time, as long as these nodes are within its charging range. Under this setting, we ask the following fundamental questions: 1) How will a multi-node charging technology affect the WCV’s travel path, charging time, and flow routing inside the network? 2) How can such multi-node charging technology address the scalability problem in a dense WSN?

To best address these two questions, we propose to take a formal optimization approach. Given the limitation of a WCV’s charging range, we propose a cellular structure that partitions a two-dimensional plane into hexagonal cells (similar to cellular structure for cellular telecommunications). To charge all sensor nodes in a cell, the WCV only needs to visit the center of the cell. Based on a general energy charging model, we formulate a joint optimization problem for traveling path, flow routing, and charging time, with the objective of maximizing the ratio of the WCV’s vacation time (time spent at its home service station) over the cycle time. We show that our optimization problem

is a nonlinear program (NLP) and is NP-hard in general. By employing discretization and a novel *Reformulation-Linearization Technique* (RLT), we develop a provably near-optimal solution for any desired level of accuracy. Using numerical results, we show that our solution can indeed improve significantly upon single-node charging technology and effectively address the charging scalability problem in a dense WSN.

The rest of this paper is organized as follows. In Section II, we review related work on wireless energy transfer. In Section III, we describe the mathematical model in our study. Section IV presents a formulation of our optimization problem and discusses several interesting properties associated with an optimal solution. In Section V, we develop a near-optimal solution, and in Section VI, we prove its near-optimality. In Section VII, we present numerical results to demonstrate our solution. Section VIII concludes this paper.

II. RELATED WORK

Current wireless energy transfer technologies can be classified into three categories, namely, inductive coupling, electromagnetic radiation, and magnetic resonant coupling. Inductive coupling works by having a primary coil at a source generate a varying magnetic field that induces a voltage across the terminals of a secondary coil at the receiver. Although this wireless energy transfer technology has found a number of successful applications in portable electronic devices (e.g., electric toothbrush, RFID tags [6], [11], medical implants [24]), it is not suitable for charging a wireless sensor node. This is because it has stringent requirements such as close contact and accurate alignment in charging direction, etc.

Electromagnetic radiation is a radiative technology that transfers power on a radio frequency (e.g., 850–950 MHz [17] or 902–928 MHz [19], both with a center frequency of 915 MHz). Under such radiative technology, an RF transmitter broadcasts radio waves in the 915-MHz ISM band, and an RF receiver tunes to the same frequency band to harvest radio power. Radiative technology has a number of difficulties in transferring energy. First, it requires uninterrupted LOS and is sensitive to any obstruction between an energy source and a receiver. Second, for omnidirectional radiation, the energy transfer efficiency is very low. Radiative technology has been explored for energy harvesting in a WSN [8], [16], [23]. In [8], He *et al.* found that a receiver could only obtain about 1.5 mW power when it is 30 cm away from the RF transmitter, with about 1.5% energy transfer efficiency. Similar experimental findings were also reported in [16] and [23]. Although this technology may alleviate the energy problem in a WSN to some extent, its applications are very limited, mainly due to its low energy transfer efficiency.

The third category of wireless energy transfer technology is magnetic resonant coupling [12], which is regarded as a major breakthrough in our time and is the technology that we explore in this paper. This technology works by having magnetic resonant coils operating at the same resonant frequency (i.e., 9.9 MHz [12] or 6.5 MHz [13]), so that energy can be transferred efficiently from a source coil to a receiver coil via nonradiative magnetic resonant induction. Compared to electromagnetic radiation, magnetic resonant coupling has the advantages of offering much higher energy transfer efficiency

even under omnidirection, not requiring LOS, and being insensitive to the neighboring environment. Although efficient energy transfer in the preliminary experiments by Kurs *et al.* is still limited by meter-range (e.g., 2 m with 60% efficiency [13]), there have been rapid advances in magnetic resonant coupling to make it suitable for commercial applications [26] such as mobile devices (e.g., cell phones, tablets, laptops) and electric/hybrid vehicles.

In [25], we presented a study on how to exploit magnetic resonant coupling for a WSN. We showed that by having a WCV visit and charge each sensor node individually in the network, a WSN can remain operational forever (i.e., infinite lifetime). An open problem that remained in [25] is scalability, i.e., how can this wireless charging technology cope with growing node density of a WSN? This is the focus of this paper.

The scope of this paper has fundamental differences from those in [7] and [20], which studied base-station movement problem. First, the WCV discussed in this paper serves a completely different purpose from a mobile base station. The WCV is employed to charge sensor nodes, while a mobile base station is used as a sink node for all data that is collected from sensor nodes. Note that in this paper, we have both a *mobile* WCV and a *fixed* base station. Second, the goal of this paper is to have each sensor node in the network never run out of energy, i.e., infinite lifetime. On the other hand, the goal of [7] and [20] is to maximize lifetime, under a finite energy constraint at each sensor node. Due to these differences, existing solution approaches for a mobile base station such as those in [7] and [20] cannot be applied to the problem in this paper.

III. MATHEMATICAL MODELING

A. Cellular Structure and Energy Charging Behavior

We consider a set of sensor nodes \mathcal{N} distributed over a two-dimensional area (see Fig. 1). Each sensor node has a battery capacity of E_{\max} and is fully charged initially. Denote E_{\min} as the minimum energy at a sensor node battery for it to be operational. To support wireless power transfer, we assume that a receiver coil is installed on each sensor node.² Each sensor node i generates sensing data with a rate R_i (in b/s), $i \in \mathcal{N}$. Within the sensor network, there is a fixed base station (B), which is the sink node for all data generated by all sensor nodes. Multihop data routing is employed for forwarding all data streams to the base station.

To recharge the battery at each sensor node, a mobile WCV is employed. The WCV starts at the service station (S), and travels (at a speed of V m/s) to various spots inside the network to charge batteries of sensor nodes. As discussed, the WCV can charge multiple nodes simultaneously as long as they are within its charging range, denoted as D . The charging range D is determined by having the power reception rate at a sensor node be at least over a threshold (denoted as δ). The power reception rate at a sensor node i , denoted as U_i , is a distance-dependent parameter and decreases with distance between itself and the WCV. When a sensor node is more than a distance of D away from the WCV, we assume its power reception rate is too low to make

²To install receiver coils, there is one-time device cost. Note that a receiver coil receives energy passively, and thus no energy will be consumed for running a receiver coil on sensor nodes.

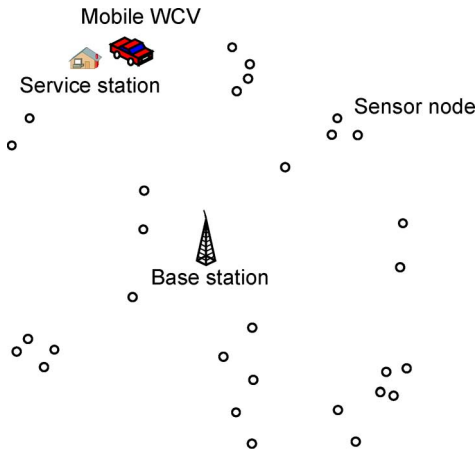


Fig. 1. Example sensor network with a mobile WCV.

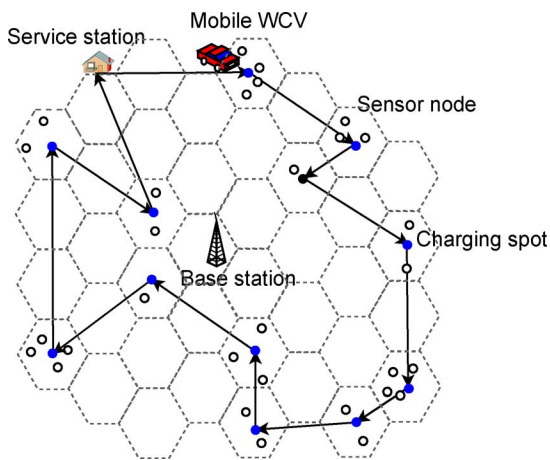


Fig. 2. Example sensor network with a mobile WCV. Solid dots represent cell centers, and empty circles represent sensor nodes.

magnetic resonant coupling work properly at the sensor node's battery. D is determined by the state of the art in wireless energy transfer research [13], which will be given in Section VII.

Ideally, we would like to solve a problem where the WCV can stop anywhere within the two-dimensional plane and charges sensor nodes wirelessly. However, this problem has an infinite number of possible locations, thus leading to an infinite size of search space. To make a concrete step in understanding the multi-node charging technology, we simplify the problem by introducing a logical cellular structure and assume the WCV can only stop at the center of a cell. Specifically, we partition the two-dimensional plane with hexagonal cells with a side length of D (see Fig. 2). Therefore, when the WCV makes a stop at the center of a cell, all sensor nodes in the cell can be charged simultaneously. We ignore the edge effect where a sensor node residing outside the cell but inside a circle with a radius of D can still be charged from this cell. Note that such omission of overcharging will not affect the feasibility of our solution.

Under the cellular structure, denote D_i the distance from node i to its cell center. Then, node i 's power reception rate is $U_i = \mu(D_i) \cdot U_{\text{Full}}$, where U_{Full} is the full output power from WCV for a single sensor node and $\mu(D_i)$ is the efficiency of wireless power transfer. Note that $\mu(D_i)$ is a decreasing function of D_i and $0 \leq \mu(D_i) \leq 1$. Although mutual coupling among

 TABLE I
 NOTATION

Symbol	Definition
a_k	Arrival time of the WCV at cell k in the first cycle
B	Base station
C_{ij} (or C_{iB})	Energy consumption for transmitting one unit of data rate from node i to node j (or the base station B)
D	WCV's charging range
D_i	Distance from node i to its cell center
D_{ij} (or D_{iS})	Distance from node i to node j (or the service station S)
D_P	The distance of path P
D_{TSP}	The minimum traveling distance in a path P
E_{max}	Full battery capacity at a sensor node
E_{min}	Minimum energy required to keep a sensor node operational
$e_i(t)$	Energy level of sensor node i at time t
f_{ij} (or f_{iB})	Flow rate from sensor node i to sensor node j (or base station B)
L	Number of points used in discretizing η_k
\mathcal{N}	The set of sensor nodes in the network
\mathcal{N}_k	The set of sensor nodes in the k -th cell
P	The traveling path of the WCV in a cycle
p_i	Energy consumption rate at sensor node i
\mathcal{Q}	The set of cells with at least one sensor node
R_i	Data rate generated at sensor node i
S	Service station
U_{Full}	Maximum output power from the WCV to charge a single sensor node
U_i	Power reception rate at sensor node i
V	Traveling speed of the WCV
α	Path loss index
β_1	A constant in energy consumed for data transmission
β_2	A coefficient in energy consumed for data transmission
ρ	Power consumption coefficient for receiving data
δ	A threshold for a sensor's power reception rate
ϵ	Targeted performance gap ($0 < \epsilon \ll 1$)
η_k	The ratio of the charging time at cell k to the cycle time
η_{kl}	Discrete points used for discretizing η_k
η_{vac}	The ratio of the vacation time to the cycle time
π_k	The k -th cell traversed by the WCV along path P
τ	Cycle time
τ_k	The time that the WCV stays at the center of cell k
τ_{vac}	Vacation time on a path
τ_P	WCV's traveling time on path P in a cycle
τ_{TSP}	Minimum traveling time of the WCV in a cycle
z_{kl}	A binary variable indicating whether or not η_{kl} is chosen, $k \in \mathcal{Q}, l = 0, \dots, L$
γ_{ikl}	$\gamma_{ikl} \triangleq z_{kl} \cdot p_i$
$\mu(D_i)$	The power transfer efficiency from the WCV to a sensor node that is at a distance D_i away

receiving coils at sensor nodes may produce interference that affects U_i , it has been shown in [1] that such effect can be properly handled by adjusting the resonant and driving frequencies according to the couplings among the receiving coils.

Under this setting, we are interested in finding out how the WCV should travel and charge from these cell centers so that: 1) none of the sensor nodes run out of energy; and 2) some performance objective can be optimized. In the rest of this section, we present a mathematical characterization of the WCV's traveling path and cycle time (Section III-B), data flow routing and energy consumption model (Section III-C), and energy dynamics at a sensor node (Section III-D). Table I lists notation used in this paper.

B. WCV Traveling Path and Cycle Time

Denote \mathcal{Q} as the set of hexagonal cells containing at least one sensor node (see Fig. 3). Re-index these cells in \mathcal{Q} as

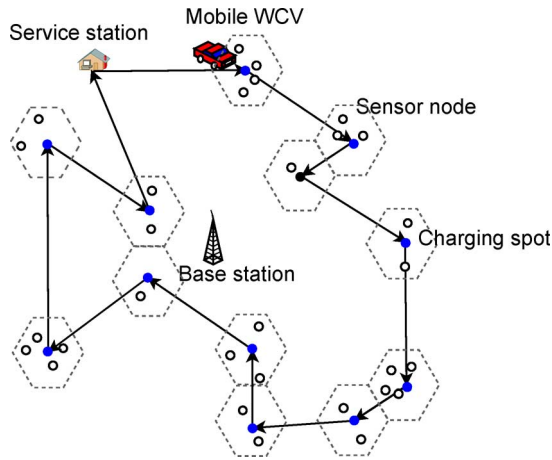


Fig. 3. Example sensor network with a WCV. Only those cells with sensor nodes are shown in this figure.

$k = 1, 2, \dots, |\mathcal{Q}|$ and denote \mathcal{N}_k the set of sensor nodes in the k th cell. Then, $\mathcal{N} = \bigcup_{k \in \mathcal{Q}} \mathcal{N}_k$.

Denote τ_k as the time that the WCV stays at the center of cell $k \in \mathcal{Q}$. Throughout τ_k , the WCV recharges all sensor nodes within this cell simultaneously via multi-node charging technology [13]. After τ_k , the WCV leaves the current cell and travels to the next cell on its path. In our formulation, we assume that the WCV visits a cell only once during a cycle. Denote $P = (\pi_0, \pi_1, \dots, \pi_{|\mathcal{Q}|}, \pi_0)$ as the physical path traversed by the WCV during a cycle, which starts from and ends at the service station (i.e., $\pi_0 = S$), and the k th cell traversed by the WCV along path P is π_k , $1 \leq k \leq |\mathcal{Q}|$. Denote D_P as the physical distance of path P and $\tau_P = D_P/V$ as the time spent for traveling over distance D_P .

After the WCV visits the $|\mathcal{Q}|$ cells in the network, it will return to its service station to be serviced (e.g., replacing its battery, taking a vacation) and get ready for the next trip. We call this resting period *vacation time*, denoted by τ_{vac} . Denote τ as the time of a cycle spent by the WCV. Then, this cycle time τ can be written as

$$\tau = \tau_P + \tau_{\text{vac}} + \sum_{k \in \mathcal{Q}} \tau_k \quad (1)$$

where $\sum_{k \in \mathcal{Q}} \tau_k$ is the total amount of time the WCV spends for battery charging. We assume that the WCV has sufficient energy to charge all sensor nodes in a cycle.

C. Data Flow Routing and Energy Consumption

To model multihop data routing, denote f_{ij} and f_{iB} the flow rates from sensor node i to sensor node j and the base station B , respectively. Then, we have the following flow balance constraint at each sensor node i :

$$\sum_{k \in \mathcal{N}}^{k \neq i} f_{ki} + R_i = \sum_{j \in \mathcal{N}}^{j \neq i} f_{ij} + f_{iB} \quad (i \in \mathcal{N}). \quad (2)$$

Although both flow routing and flow rates are part of our optimization problem, we assume they do not change with time.

In this paper, we use the following energy consumption model at each sensor node [9]. To transmit a flow rate of f_{ij} from node i to node j , the transmission power is $C_{ij} \cdot f_{ij}$, where C_{ij}

is the rate of energy consumption for transmitting one unit of data from node i to node j . C_{ij} is modeled as

$$C_{ij} = \beta_1 + \beta_2 D_{ij}^\alpha$$

where D_{ij} is the distance between nodes i and j , β_1 is a distance-independent constant term, β_2 is a coefficient of the distance-dependent term, and α is the path-loss index. Similarly, denote C_{iB} as the rate of energy consumption for transmitting one unit of data from node i to the base station B . Then, the aggregate energy consumption rate for transmission at node i is $\sum_{j \in \mathcal{N}}^{j \neq i} C_{ij} \cdot f_{ij} + C_{iB} \cdot f_{iB}$.

The energy consumption rate for reception at node i is modeled as $\rho \sum_{k \in \mathcal{N}}^{k \neq i} f_{ki}$, where ρ is the rate of energy consumption for receiving one unit of data.

Denote p_i as the energy consumption rate at sensor node $i \in \mathcal{N}$, which includes energy consumption for transmission and reception. We have

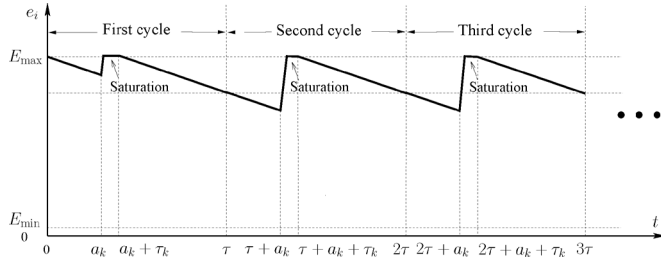
$$p_i = \rho \sum_{k \in \mathcal{N}}^{k \neq i} f_{ki} + \sum_{j \in \mathcal{N}}^{j \neq i} C_{ij} f_{ij} + C_{iB} f_{iB} \quad (i \in \mathcal{N}). \quad (3)$$

D. Energy Dynamics at a Sensor Node

In Section III-B, we discussed the WCV's behavior over a cycle time τ , during which the WCV starts from the service station, travels to those cells with sensor nodes, and returns to the service station (see Fig. 3).

Multi-Node Charging Versus Single-Node Charging: In our previous work in [25], we considered a WCV visiting each node and charging it individually. In that context, we introduced a concept called *renewable energy cycle*, during which the energy level at each node exhibits a periodic behavior with a cycle time τ . Specifically, the energy level of a sensor node exhibits a renewable energy cycle if it meets the following two requirements: 1) it starts and ends with the same energy level over a period of τ ; and 2) it never falls below E_{\min} . A central idea in achieving a renewable energy cycle in [25] is that the amount of energy being charged to a node is equal to the amount of energy that the node expends in a cycle. However, such an idea cannot be extended to our multi-node charging context here. This is because, for each node in the same cell, its remaining energy level (when the WCV arrives at the cell) differs, as do energy charging rate and consumption rate at each node. As a result, nodes in the same cell will not complete their battery charging at the same time, and those nodes that finish early will run into a "saturation" state (i.e., battery level remains at E_{\max}) until the WCV departs this cell (see Fig. 4). Due to such this "saturation" phenomena, the idea of achieving a renewable energy cycle cannot be applied here.

Cell-Based Energy Constraints: We now develop constraints to capture the saturation phenomena while ensuring that the energy level of each node never falls below E_{\min} . Denote $e_i(t)$ as node i 's energy level at time t . The energy curve of node $i \in \mathcal{N}_k$ in a cell k for the first three cycles is shown in Fig. 4. For any cycle, we see that there can be only three possible slopes: 1) a slope of $-p_i$ when the WCV is not in node i 's cell; 2) a slope of $(U_i - p_i)$ when the WCV is at node i 's cell and is charging


 Fig. 4. Energy level of node $i \in \mathcal{N}_k$ during the first three cycles.

node i at rate U_i ³; and 3) a slope of 0 (i.e., saturation period) when node i stays at E_{\max} while the WCV is still charging.

Denote a_k as the arrival time of the WCV at cell k in the first cycle. Denote $D_{\pi_0 \pi_1}$ as the distance between the service station and the first cell visited along P and $D_{\pi_l \pi_{l+1}}$ as the distance between the l th and $(l+1)$ th cells, respectively. Then, we have

$$a_{\pi_k} = \sum_{l=0}^{k-1} \frac{D_{\pi_l \pi_{l+1}}}{V} + \sum_{l=1}^{k-1} \tau_{\pi_l}, \quad k = 1, 2, \dots, |\mathcal{Q}|.$$

Note that $e_i(m\tau + a_k)$, $m \in \mathbb{N}$, is a local minimum for $e_i(t)$. To have $e_i(t) \geq E_{\min}$ for all $t \geq 0$, it is sufficient to have

$$e_i(m\tau + a_k) = e_i(m\tau) - a_k \cdot p_i \geq E_{\min}$$

for all $m \in \mathbb{N}$, $i \in \mathcal{N}_k$, $k \in \mathcal{Q}$.

When $m = 0$, $e_i(a_k) = e_i(0) - a_k \cdot p_i = E_{\max} - a_k \cdot p_i$. For $e_i(a_k) \geq E_{\min}$, we must have

$$E_{\max} - a_k \cdot p_i \geq E_{\min} \quad (i \in \mathcal{N}_k, k \in \mathcal{Q}). \quad (4)$$

When $m \geq 1$

$$\begin{aligned} e_i(m\tau + a_k) &= e_i(m\tau) - a_k \cdot p_i \\ &= e_i((m-1)\tau + a_k + \tau_k) \\ &\quad - \{m\tau - [(m-1)\tau + a_k + \tau_k]\} \cdot p_i \\ &\quad - a_k \cdot p_i \\ &= e_i((m-1)\tau + a_k + \tau_k) - (\tau - \tau_k) \cdot p_i \\ &\leq E_{\max} - (\tau - \tau_k) \cdot p_i \end{aligned} \quad (5)$$

where the last inequality holds since e_i cannot exceed E_{\max} . For (5), if $e_i(m\tau + a_k) \geq E_{\min}$ for all $m \geq 1$, then we must have

$$E_{\max} - (\tau - \tau_k) \cdot p_i \geq E_{\min} \quad (i \in \mathcal{N}_k, k \in \mathcal{Q}). \quad (6)$$

Now we show that once (6) holds, (4) must also hold. Therefore, we can remove (4) in the formulation. To see this, we have $a_k + \tau_k < \tau$, which leads to $E_{\max} - a_k \cdot p_i > E_{\max} - (\tau - \tau_k) \cdot p_i$.

Note that (6) is a necessary condition for $e_i(t) \geq E_{\min}$. The following is a second necessary condition for $e_i(t) \geq E_{\min}$:

$$\tau \cdot p_i - U_i \cdot \tau_k \leq 0 \quad (i \in \mathcal{N}_k, k \in \mathcal{Q}) \quad (7)$$

³Note that it is necessary to have $U_i \geq p_i$ for $i \in \mathcal{N}$ to achieve a feasible solution.

which says that $U_i \cdot \tau_k$, the amount of energy being charged to node $i \in \mathcal{N}_k$ during the time period of τ_k , must be greater than or equal to $\tau \cdot p_i$, the amount of energy consumed during the cycle. Equation (7) can be easily proved by showing that if $\tau \cdot p_i - U_i \cdot \tau_k > 0$, then $e_i(t)$ will fall below E_{\min} eventually at some time t .

We have shown that (6) and (7) are necessary conditions for $e_i(t) \geq E_{\min}$. It turns out that they are also sufficient conditions. We state this result in the following lemma.

Lemma 1: $e_i(t) \geq E_{\min}$ for all $t \geq 0$, $i \in \mathcal{N}$, if and only if both constraints (6) and (7) are satisfied.

The proof of Lemma 1 is given in the Appendix.

The following corollary follows from the proof of Lemma 1.

Corollary 1.1: When the WCV departs cell k , $k \in \mathcal{Q}$, each sensor node $i \in \mathcal{N}_k$ is fully charged to E_{\max} .

IV. PROBLEM FORMULATION AND PROPERTIES

Based on the constraints that we have discussed in Section III, we consider optimizing some global performance objective. In particular, we would like to minimize energy consumption of the entire system, which encompasses all energy consumption at the WCV.⁴ Since the energy consumed to carry the WCV to move along P is the dominant source of energy consumption (when compared to its wireless charging to sensor nodes), we aim to minimize the fraction of time that the WCV is outside its service station, i.e., $\frac{\tau_P + \sum_{k \in \mathcal{Q}} \tau_k}{\tau}$.⁵ It is interesting that, by (1), minimizing $\frac{\tau_P + \sum_{k \in \mathcal{Q}} \tau_k}{\tau}$ is equivalent to maximizing $\frac{\tau_{\text{vac}}}{\tau}$, which is the percentage of time that the WCV is on vacation at its service station.

Mathematically, this is a very challenging objective, as it involves a ratio of two variables. Therefore, a successful solution to this optimization problem will help pave the way to solve many other optimization problems with simpler objectives.

We now summarize our optimization problem as follows:

$$\begin{aligned} \max \quad & \frac{\tau_{\text{vac}}}{\tau} \\ \text{s.t.} \quad & \text{Time constraint: (1);} \\ & \text{Flow routing constraints: (2);} \\ & \text{Energy consumption model: (3);} \\ & \text{Cell-based energy constraints: (6), (7).} \\ & \tau, \tau_P, \tau_{\text{vac}}, \tau_k, f_{ij}, f_{iB} \geq 0 \quad (i, j \in \mathcal{N}, i \neq j) \\ & 0 \leq p_i \leq U_i \quad (i \in \mathcal{N}). \end{aligned}$$

In this problem, time intervals τ , τ_P , τ_{vac} , and τ_k , flow rates f_{ij} and f_{iB} , and power consumption rate p_i are optimization variables; R_i , ρ , C_{ij} , C_{iB} , U_i , E_{\max} , and E_{\min} are constants. Note that τ_P can be determined once the traveling path P is determined.

This problem is an NLP, with nonlinear objective ($\frac{\tau_{\text{vac}}}{\tau}$) and nonlinear terms ($\tau \cdot p_i$ and $\tau_k \cdot p_i$) in constraints (6) and (7).

⁴Note that except for their initial energy, the energy consumed in the sensor network comes from the WCV.

⁵We include the energy consumed at a WCV when it makes stops at a cell because the WCV's engine may be still on.

An NLP is NP-hard in general. Nevertheless, we can still find several useful properties associated with an optimal solution.

Property 1: In an optimal solution with the maximal $\frac{\tau_{\text{vac}}}{\tau}$, the WCV must move along the shortest Hamiltonian cycle that connects the service station and the centers of cells $k \in \mathcal{Q}$. If the shortest Hamiltonian cycle is not unique, then any shortest Hamiltonian cycle can achieve the same optimal objective. Furthermore, the WCV can follow either clockwise or counter-clockwise direction of the shortest Hamiltonian cycle, both of which will achieve the same optimal objective.

A proof of this property can be developed based on contradiction. That is, if there is an optimal solution where the WCV does not move along the shortest Hamiltonian cycle, then we can construct a new solution with the WCV moving along the shortest Hamiltonian cycle and with an improved objective. Since it shares a similar idea to a proof in [25], we omit it here to conserve space.

The shortest Hamiltonian cycle can be obtained by solving the well known Traveling Salesman Problem (TSP) [2], [4]. Denote D_{TSP} as the total path distance for the shortest Hamiltonian cycle and $\tau_{\text{TSP}} = D_{\text{TSP}}/V$. Then, (1) becomes

$$\tau - \sum_{k \in \mathcal{Q}} \tau_k - \tau_{\text{vac}} = \tau_{\text{TSP}}. \quad (8)$$

The solution to our problem becomes $\varphi = (P_{\text{TSP}}, \tau, \tau_{\text{TSP}}, \tau_{\text{vac}}, \tau_k, f_{ij}, f_{iB}, p_i)$. Since the optimal traveling path is determined, we simplify the notation for φ as $\varphi = (\tau, \tau_{\text{vac}}, \tau_k, f_{ij}, f_{iB}, p_i)$.

For (8), we divide both sides by τ and have $1 - \sum_{k \in \mathcal{Q}} \frac{\tau_k}{\tau} - \frac{\tau_{\text{vac}}}{\tau} = \tau_{\text{TSP}} \cdot \frac{1}{\tau}$. We define $\eta_{\text{vac}} = \frac{\tau_{\text{vac}}}{\tau}$, where η_{vac} represents the ratio of the vacation time to the entire cycle time and is our objective function in the optimization problem. Similarly, we define $\eta_k = \frac{\tau_k}{\tau}$, for $k \in \mathcal{Q}$, and $h = \frac{1}{\tau}$, where η_k represents the ratio of the charging time at cell k to the entire cycle time. Then, (8) is written as $1 - \sum_{k \in \mathcal{Q}} \eta_k - \eta_{\text{vac}} = \tau_{\text{TSP}} \cdot h$, or equivalently, $h = \frac{1 - \sum_{k \in \mathcal{Q}} \eta_k - \eta_{\text{vac}}}{\tau_{\text{TSP}}}$.

Similarly, by dividing both sides by τ , replacing $\frac{\tau_k}{\tau}$ with η_k , and replacing $\frac{1}{\tau}$ with $\frac{1 - \sum_{k \in \mathcal{Q}} \eta_k - \eta_{\text{vac}}}{\tau_{\text{TSP}}}$, (6) and (7) can be reformulated as

$$(1 - \eta_k) \cdot p_i \leq (E_{\text{max}} - E_{\text{min}}) \cdot \frac{1 - \sum_{j \in \mathcal{Q}} \eta_j - \eta_{\text{vac}}}{\tau_{\text{TSP}}} \quad (i \in \mathcal{N}_k, k \in \mathcal{Q})$$

$$p_i - U_i \cdot \eta_k \leq 0 \quad (i \in \mathcal{N}_k, k \in \mathcal{Q}). \quad (9)$$

We can rewrite (9) as

$$\eta_{\text{vac}} \leq 1 - \sum_{j \in \mathcal{Q}} \eta_j - \frac{\tau_{\text{TSP}}}{E_{\text{max}} - E_{\text{min}}} (1 - \eta_k) \cdot p_i \quad (i \in \mathcal{N}_k, k \in \mathcal{Q}).$$

Now our problem is reformulated as follows:

OPT

$$\begin{aligned} \max \quad & \eta_{\text{vac}} \\ \text{s.t.} \quad & \sum_{j \in \mathcal{N}}^{j \neq i} f_{ij} + f_{iB} - \sum_{k \in \mathcal{N}}^{k \neq i} f_{ki} = R_i \quad (i \in \mathcal{N}) \\ & \rho \cdot \sum_{k \in \mathcal{N}}^{k \neq i} f_{ki} + \sum_{j \in \mathcal{N}}^{j \neq i} C_{ij} \cdot f_{ij} + C_{iB} \cdot f_{iB} - p_i = 0 \quad (i \in \mathcal{N}) \end{aligned}$$

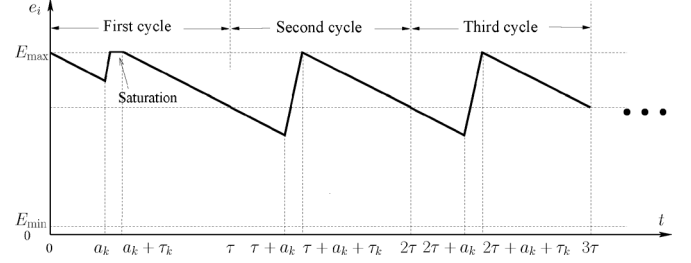


Fig. 5. Energy level of an equilibrium node $i \in \mathcal{N}_k$ in the first three cycles.

$$\eta_{\text{vac}} \leq 1 - \sum_{j \in \mathcal{Q}} \eta_j - \frac{\tau_{\text{TSP}}}{E_{\text{max}} - E_{\text{min}}} (1 - \eta_k) \cdot p_i \quad (i \in \mathcal{N}_k, k \in \mathcal{Q}) \quad (10)$$

$$p_i - U_i \cdot \eta_k \leq 0 \quad (i \in \mathcal{N}_k, k \in \mathcal{Q}) \quad (11)$$

$$f_{ij}, f_{iB} \geq 0, 0 \leq p_i \leq U_i, 0 \leq \eta_k, \eta_{\text{vac}} \leq 1 \quad (i, j \in \mathcal{N}, i \neq j).$$

In this problem, f_{ij} , f_{iB} , p_i , η_{vac} , and η_k are optimization variables; R_i , ρ , C_{ij} , C_{iB} , U_i , E_{max} , E_{min} , and τ_{TSP} are constants. Once we obtain a solution to problem OPT, we can recover τ , τ_k , and τ_{vac} as follows:

$$\tau = \frac{\tau_{\text{TSP}}}{1 - \sum_{k \in \mathcal{Q}} \eta_k - \eta_{\text{vac}}} \quad (12)$$

$$\tau_k = \tau \cdot \eta_k \quad (13)$$

$$\tau_{\text{vac}} = \tau \cdot \eta_{\text{vac}}. \quad (14)$$

In an optimal solution to OPT, we show that there exists at least one *bottleneck node*, which is defined as the node whose energy level drops exactly to E_{min} upon WCV's arrival.

Property 2: In an optimal solution to OPT, there exists at least one bottleneck node in the network.

The proof of Property 2 is given in the Appendix. Based on Corollary 1.1, we know that when the WCV departs a cell k , $k \in \mathcal{Q}$, each sensor node in this cell is fully charged to E_{max} . Furthermore, some nodes may experience saturation state during each cycle. The following property says that in an optimal solution, at least one sensor node in each cell $k \in \mathcal{Q}$ will have saturation-free cycles except its initial first cycle (see Fig. 5).

Property 3: In an optimal solution to OPT, there exists at least one node in each cell $k \in \mathcal{Q}$ such that, starting from the second cycle, the amount of energy reception at the node is the same as the amount of energy consumption in the cycle.

The proof of Property 3 is given in the Appendix. We call the node in Property 3 an *equilibrium node*. Note that the definition of equilibrium node is different from the bottleneck node.

V. NEAR-OPTIMAL SOLUTION

A. Approach

Problem OPT is an NLP, with bilinear terms ($\eta_k \cdot p_i$) in constraints (10). This nonlinear (bilinear) program is nonconvex [5] and cannot be solved by existing off-the-shelf solvers.

In this section, we convert the NLP to a mixed-integer linear program (MILP), which can then be solved efficiently by an off-the-shelf solver such as CPLEX [10]. First, we discretize variable η_k in the bilinear term $\eta_k \cdot p_i$ using binary variables. This converts problem OPT to a 0-1 mixed-integer nonlinear

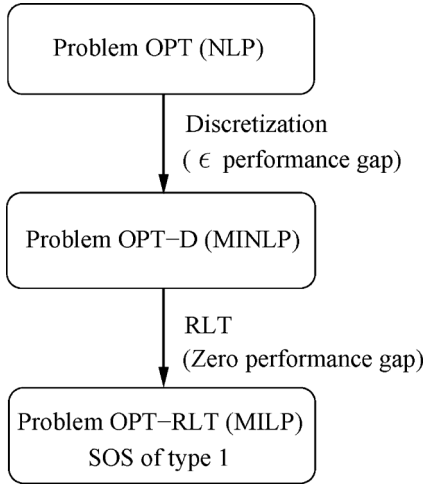


Fig. 6. Flowchart of our solution roadmap.

program (MINLP). By exploiting the special structures of the 0-1 MINLP, we employ a powerful technique called *Reformulation-Linearization Technique* [21] to eliminate all bilinear terms. Subsequently, we have a 0-1 MILP, and we show that this new 0-1 MILP and the 0-1 MINLP have zero performance gap. This MILP has special ordered sets (SOSs), which can be efficiently solved by CPLEX solver [10]. We quantify performance gap (due to discretization) and prove near-optimality of our solution. A flowchart of our solution roadmap is given in Fig. 6.

B. Discretization

As a first step to reformulate the NLP to MILP, we consider the bilinear term $\eta_k \cdot p_i$. Since η_k is a continuous variable within $[0, 1]$, we discretize it by using $L + 1$ discrete points $\eta_{kl} = \frac{l}{L}$, $l = 0, 1, \dots, L$. Then, we write

$$\eta_k = \sum_{l=0}^L \eta_{kl} \cdot z_{kl}, \quad k \in \mathcal{Q} \quad (15)$$

$$\sum_{l=0}^L z_{kl} = 1, \quad k \in \mathcal{Q} \quad (16)$$

where z_{kl} is a binary variable that indicates whether or not η_{kl} is chosen. By (15), the term $\eta_k \cdot p_i$ in (10) can be rewritten as $\eta_k \cdot p_i = \sum_{l=0}^L \eta_{kl} \cdot z_{kl} \cdot p_i$, which remains a bilinear term involving binary variables z_{kl} , $l = 1, 2, \dots, L$. This makes the problem a 0-1 MINLP, which is formulated as follows:

OPT-D

$$\begin{aligned} \max \quad & \eta_{\text{vac}} \\ \text{s.t.} \quad & \sum_{j \in \mathcal{N}}^{j \neq i} f_{ij} + f_{iB} - \sum_{k \in \mathcal{N}}^{k \neq i} f_{ki} = R_i \quad (i \in \mathcal{N}) \\ & \rho \cdot \sum_{k \in \mathcal{N}}^{k \neq i} f_{ki} + \sum_{j \in \mathcal{N}}^{j \neq i} C_{ij} \cdot f_{ij} + C_{iB} \cdot f_{iB} - p_i = 0 \quad (i \in \mathcal{N}) \end{aligned}$$

$$\begin{aligned} \eta_{\text{vac}} \leq 1 - \sum_{j \in \mathcal{Q}} \sum_{l=0}^L \eta_{jl} \cdot z_{jl} - \frac{\tau_{\text{TSP}}}{E_{\text{max}} - E_{\text{min}}} \\ \cdot (p_i - \sum_{l=0}^L \eta_{kl} \cdot z_{kl} \cdot p_i) \quad (i \in \mathcal{N}_k, k \in \mathcal{Q}) \quad (17) \end{aligned}$$

$$p_i - U_i \sum_{l=0}^L \eta_{kl} \cdot z_{kl} \leq 0 \quad (i \in \mathcal{N}_k, k \in \mathcal{Q}) \quad (18)$$

$$\begin{aligned} \sum_{l=0}^L z_{kl} = 1 \quad (k \in \mathcal{Q}) \\ f_{ij}, f_{iB} \geq 0, 0 \leq p_i \leq U_i, 0 \leq \eta_{\text{vac}} \leq 1 \\ (i, j \in \mathcal{N}, i \neq j) \\ z_{kl} \in \{0, 1\} \quad (i \in \mathcal{N}_k, k \in \mathcal{Q}, l = 0, \dots, L). \end{aligned}$$

C. Reformulation and Linearization

To remove the nonlinear terms $z_{kl} \cdot p_i$ in the 0-1 MINLP, we employ a powerful technique called RLT as follows. Define

$$\gamma_{ikl} \triangleq z_{kl} \cdot p_i, \quad i \in \mathcal{N}_k, k \in \mathcal{Q}, l = 0, \dots, L. \quad (19)$$

Then, $\sum_{l=0}^L \eta_{kl} \cdot z_{kl} \cdot p_i$ can be rewritten as $\sum_{l=0}^L \eta_{kl} \cdot z_{kl} \cdot p_i = \sum_{l=0}^L \eta_{kl} \cdot \gamma_{ikl}$, $i \in \mathcal{N}_k, k \in \mathcal{Q}$.

To replace the nonlinear constraint (19), we need to add RLT constraints, which are linear. The new linear constraints are generated by multiplying existing linear constraints for variables z_{kl} and p_i , which are $1 - \sum_{l=0}^L z_{kl} = 0$, $z_{kl} \geq 0$, $p_i \geq 0$ and $U_i - p_i \geq 0$. It is worth pointing out that RLT in [22] typically refers to multiplying each pair of these constraints (i.e., reformulation) and generating linear constraints via variable substitution (i.e., linearization). For our problem, this will produce several redundant or null constraints. To reduce such redundancy, we exploit a special structure of our problem, i.e., the presence of equality constraints $1 - \sum_{l=0}^L z_{kl} = 0$. It is only necessary to multiply these constraints (and $z_{kl} \geq 0$) by $p_i \geq 0$ and $U_i - p_i \geq 0$. Multiplying $1 - \sum_{l=0}^L z_{kl} = 0$ by $p_i \geq 0$ gives us

$$\sum_{l=0}^L z_{kl} \cdot p_i = p_i, \quad i \in \mathcal{N}_k, k \in \mathcal{Q}$$

which can be written as

$$\sum_{l=0}^L \gamma_{ikl} = p_i, \quad i \in \mathcal{N}_k, k \in \mathcal{Q}. \quad (20)$$

Multiplying $1 - \sum_{l=0}^L z_{kl} = 0$ by $U_i - p_i \geq 0$ simply produces constraint (20), or $1 - \sum_{l=0}^L z_{kl} = 0$ if $U_i - p_i > 0$, or $U_i - p_i = 0$, none of which is new.

Multiplying $p_i \geq 0$ and $U_i - p_i \geq 0$ by $z_{kl} \geq 0$, respectively, we have the following RLT constraints:

$$0 \leq z_{kl} \cdot p_i \leq U_i z_{kl}, \quad i \in \mathcal{N}_k, k \in \mathcal{Q}, l = 0, \dots, L$$

which can be written as

$$0 \leq \gamma_{ikl} \leq U_i z_{kl}, \quad i \in \mathcal{N}_k, k \in \mathcal{Q}, l = 0, \dots, L. \quad (21)$$

In summary, the new RLT constraints are (20) and (21). By substituting (19) for $z_{kl} \cdot p_i$, and adding the new RLT constraints (20) and (21), we obtain the following 0-1 MILP:

OPT-RLT

$$\begin{aligned} \max \quad & \eta_{\text{vac}} \\ \text{s.t.} \quad & \sum_{j \in \mathcal{N}}^{j \neq i} f_{ij} + f_{iB} - \sum_{k \in \mathcal{N}}^{k \neq i} f_{ki} = R_i \quad (i \in \mathcal{N}) \\ & \rho \cdot \sum_{k \in \mathcal{N}}^{k \neq i} f_{ki} + \sum_{j \in \mathcal{N}}^{j \neq i} C_{ij} \cdot f_{ij} + C_{iB} \cdot f_{iB} - p_i = 0 \quad (i \in \mathcal{N}) \end{aligned}$$

$$\eta_{\text{vac}} \leq 1 - \sum_{j \in \mathcal{Q}} \sum_{l=0}^L \eta_{jl} \cdot z_{jl} - \frac{\tau_{\text{TSP}}}{E_{\text{max}} - E_{\text{min}}} \cdot \left(p_i - \sum_{l=0}^L \eta_{kl} \cdot \gamma_{ikl} \right) \quad (i \in \mathcal{N}_k, k \in \mathcal{Q}) \quad (22)$$

$$\begin{aligned} p_i - U_i \sum_{l=0}^L \eta_{kl} \cdot z_{kl} &\leq 0 \quad (i \in \mathcal{N}_k, k \in \mathcal{Q}) \\ \sum_{l=0}^L z_{kl} &= 1 \quad (k \in \mathcal{Q}) \\ \sum_{l=0}^L \gamma_{ikl} - p_i &= 0 \quad (i \in \mathcal{N}_k, k \in \mathcal{Q}) \\ \gamma_{ikl} - U_i z_{kl} &\leq 0 \quad (i \in \mathcal{N}_k, k \in \mathcal{Q}, l = 0, \dots, L) \\ f_{ij}, f_{iB} &\geq 0, 0 \leq p_i \leq U_i, 0 \leq \eta_{\text{vac}} \leq 1 \\ &\quad (i, j \in \mathcal{N}, i \neq j) \\ \gamma_{ikl} &\geq 0, z_{kl} \in \{0, 1\} \quad (i \in \mathcal{N}_k, k \in \mathcal{Q}, l = 0, \dots, L). \end{aligned}$$

In this problem, f_{ij} , f_{iB} , p_i , η_{vac} , and γ_{ikl} are continuous variables; z_{kl} are binary variables; R_i , ρ , C_{ij} , C_{iB} , U_i , η_{kl} , E_{max} , E_{min} , and τ_{TSP} are constants. The integer variables z_{kl} , $l = 0, 1, \dots, L$, are constrained by (16) and form an SOS of type 1 (meaning that at most one of the variables in the set may be nonzero) [3]. It turns out that such a special type of MILP is particularly suitable for CPLEX solver as CPLEX can use special branching strategies to improve performance [10].

Through RLT, we have eliminated all bilinear terms in the 0-1 MINLP and have obtained a 0-1 MILP. A natural question to ask is how much the performance gap is between the optimal solutions under MINLP and MILP. The following lemma says that the performance gap between the two is zero, thus substantiating the benefits of employing RLT in our solution approach. By zero performance gap, we mean there is a bijection from the feasible region of problem OPT-D to the feasible region of problem OPT-RLT, and vice versa; any two feasible solutions corresponding to this one-to-one mapping achieve the same objective value.

Lemma 2: Problem OPT-RLT and problem OPT-D have zero performance gap.

Proof: Our proof consists of two parts.

- (i) If a solution $\psi_{\text{D}} = (f_{ij}, f_{iB}, p_i, \eta_{\text{vac}}, z_{kl})$ is feasible to problem OPT-D, then the solution $\psi_{\text{RLT}} = (f_{ij}, f_{iB}, p_i, \eta_{\text{vac}}, z_{kl}, \gamma_{ikl})$ is also feasible to problem OPT-RLT, where $\gamma_{ikl} = p_i \cdot z_{kl}$.
- (ii) If a solution $\psi_{\text{RLT}} = (f_{ij}, f_{iB}, p_i, \eta_{\text{vac}}, z_{kl}, \gamma_{ikl})$ is feasible to problem OPT-RLT, then the solution $\psi_{\text{D}} = (f_{ij}, f_{iB}, p_i, \eta_{\text{vac}}, z_{kl})$ is also feasible to problem OPT-D.

We shall prove that if both (i) and (ii) hold, then there is a bijection from the feasible region of problem OPT-D to the feasible region of problem OPT-RLT, and vice versa; for any one-to-one solution mapping between ψ_{D} and ψ_{RLT} , their objective values are the same.

For the first part, suppose we have a solution $\psi_{\text{D}} = (f_{ij}, f_{iB}, p_i, \eta_{\text{vac}}, z_{kl})$ that is feasible to problem OPT-D. To show that $\psi_{\text{RLT}} = (f_{ij}, f_{iB}, p_i, \eta_{\text{vac}}, z_{kl}, \gamma_{ikl})$ is feasible to problem OPT-RLT, we need to show that ψ_{RLT} satisfies constraints (2), (3), (16), (18), and (20)–(22). Since ψ_{D} is feasible to problem OPT-D, ψ_{D} satisfies constraints (2), (3), and (16)–(18). For ψ_{RLT} , since the values of f_{ij} , f_{iB} , p_i , and z_{kl}

A Near-Optimal Solution Procedure

1. Given a target performance gap ϵ .
2. Let $L = \lceil \frac{|\mathcal{Q}|}{\epsilon} \rceil$.
3. Solve problem OPT-RLT by CPLEX with a solution $\psi_{\text{RLT}} = (f_{ij}, f_{iB}, p_i, \eta_{\text{vac}}, z_{kl}, \gamma_{ikl})$.
4. Construct a feasible solution $\psi = (f_{ij}, f_{iB}, p_i, \eta_{\text{vac}}, \eta_k)$ to problem OPT via Lemma 3.
5. Recover τ , τ_k , τ_{vac} by (12), (13) and (14), respectively.

Fig. 7. Summary of the proposed near-optimal solution procedure.

are the same as those in ψ_{D} , ψ_{RLT} must also satisfy constraints (2), (3), (16), and (18). To verify constraint (20), we multiply (16) by p_i on both sides and have $\sum_{l=0}^L z_{kl} \cdot p_i = p_i$, or equivalently, $\sum_{l=0}^L \gamma_{ikl} = p_i$. Similarly, we can verify (21) by multiplying $0 \leq p_i \leq U_i$ by z_{kl} on both sides. From (17), since $\gamma_{ikl} = p_i \cdot z_{kl}$, (22) holds. This completes the proof of (i).

For the second part, suppose we have a solution $\psi_{\text{RLT}} = (f_{ij}, f_{iB}, p_i, \eta_{\text{vac}}, z_{kl}, \gamma_{ikl})$ that is feasible to problem OPT-RLT. To show that ψ_{D} is a feasible solution to problem OPT-D, we need to show that ψ_{D} satisfies constraints (2), (3), and (16)–(18). Since ψ_{RLT} is feasible to problem OPT-RLT, ψ_{RLT} satisfies constraints (2), (3), (16), (18), and (20)–(22). For ψ_{D} , since the value of f_{ij} , f_{iB} , p_i , and z_{kl} are the same as those in ψ_{RLT} , ψ_{D} must also satisfy constraints (2), (3), (16), and (18). Now we show that ψ_{D} satisfies (17). Since ψ_{RLT} satisfies (22), it is sufficient to show that $\gamma_{ikl} = p_i \cdot z_{kl}$. To have $\gamma_{ikl} = p_i \cdot z_{kl}$, we need to show that $\gamma_{ikl} = 0$ if $z_{kl} = 0$ and $\gamma_{ikl} = p_i$ if $z_{kl} = 1$. These are assured by (16), (20), and (21). By (16), for each $k \in \mathcal{Q}$, there is only one $z_{km} = 1$, $0 \leq m \leq L$, and other z_{kl} ($l \neq m$) equal 0. By (21), the corresponding γ_{ikl} must be 0, for all $i \in \mathcal{N}_k$, $l \neq m$. Then, by (20), the single z_{km} that equals 1 suggests $\gamma_{ikm} = p_i$, for all $i \in \mathcal{N}_k$. This completes the proof of (ii). ■

D. Recovering a Solution to the Original Problem

By now, we have obtained a solvable 0-1 MILP. Once we have an optimal solution to this MILP, the question to ask is how to recover a feasible solution to the original problem (OPT). Assuming we have a solution $\psi_{\text{RLT}} = (f_{ij}, f_{iB}, p_i, \eta_{\text{vac}}, z_{kl}, \gamma_{ikl})$ that is optimal to problem OPT-RLT, by Lemma 2, the solution $\psi_{\text{D}} = (f_{ij}, f_{iB}, p_i, \eta_{\text{vac}}, z_{kl})$ is also feasible to problem OPT-D. Based on ψ_{D} , we can construct a solution $\psi = (f_{ij}, f_{iB}, p_i, \eta_{\text{vac}}, \eta_k)$ to problem OPT by letting $\eta_k = \sum_{l=0}^L \eta_{kl} \cdot z_{kl}$, and f_{ij} , f_{iB} , p_i , and η_{vac} unchanged from ψ_{D} . Note that ψ is a feasible solution to problem OPT since the constraints in problem OPT are the same as those in problem OPT-D after we replace η_k by $\sum_{l=0}^L \eta_{kl} \cdot z_{kl}$. Since ψ is only a feasible solution to problem OPT, its objective value η_{vac} is a lower bound for problem OPT. We summarize our discussion in the following lemma.

Lemma 3: For a given optimal solution $\psi_{\text{RLT}} = (f_{ij}, f_{iB}, p_i, \eta_{\text{vac}}, z_{kl}, \gamma_{ikl})$ to problem OPT-RLT, we can construct a solution $\psi = (f_{ij}, f_{iB}, p_i, \eta_{\text{vac}}, \eta_k)$ that is feasible to Problem OPT by letting $\eta_k = \sum_{l=0}^L \eta_{kl} \cdot z_{kl}$. Furthermore, η_{vac} is a lower bound for the optimal objective value of Problem OPT.

We summarize our near-optimal solution procedure to OPT in Fig. 7.

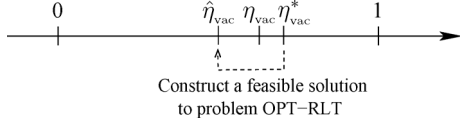


Fig. 8. Illustration of main idea in the proof of Lemma 4. η_{vac}^* is the objective value under an optimal (unknown) solution ψ^* to problem OPT. η_{vac} is the objective value under an optimal solution ψ_{RLT} to problem OPT-RLT that is obtained by solving the 0-1 MILP (OPT-RLT). $\hat{\eta}_{\text{vac}}$ is the objective value obtained by the constructed feasible solution $\hat{\psi}_{\text{RLT}}$ to problem OPT-RLT.

VI. PROOF OF NEAR-OPTIMALITY

Recall that our original problem is OPT, which is an NLP. We converted this NLP to a 0-1 MINLP via discretization (problem OPT-D) and then to a 0-1 MILP via RLT (problem OPT-RLT). We proved that problem OPT-D and problem OPT-RLT have zero performance gap. Hence, the performance gap between problems OPT and OPT-RLT could only occur during discretization.

Quantifying Performance Gap: By solving problem OPT-RLT, we obtain an optimal solution ψ_{RLT} to problem OPT-RLT. Denote ψ^* the optimal (unknown) solution to problem OPT. Denote η_{vac} the optimal objective value obtained by ψ_{RLT} and η_{vac}^* the optimal objective value obtained by ψ^* , respectively. Naturally, the gap between η_{vac} and η_{vac}^* is closely tied to L , which is the number of discrete points used in discretization. We quantify this gap in the following lemma.

Lemma 4: For a given L , we have $\eta_{\text{vac}}^* - \eta_{\text{vac}} \leq \frac{|Q|}{L}$.

Proof: We consider two cases, depending on whether $\eta_{\text{vac}} \leq \frac{|Q|}{L}$ or $\eta_{\text{vac}} > \frac{|Q|}{L}$.

Case i: Suppose $\eta_{\text{vac}} \leq \frac{|Q|}{L}$. This is the trivial case. Since $\eta_{\text{vac}} \geq 0$, we have $\eta_{\text{vac}}^* - \eta_{\text{vac}} \leq \frac{|Q|}{L}$.

Case ii: Suppose $\eta_{\text{vac}} > \frac{|Q|}{L}$. This is the most common case. The rest of the proof is devoted to this case, and its main idea is illustrated in Fig. 8. Denote $\hat{\psi}_{\text{RLT}}$ as a feasible solution to problem OPT-RLT and $\hat{\eta}_{\text{vac}}$ as the objective value under $\hat{\psi}_{\text{RLT}}$. Since η_{vac} is the objective value of an optimal solution ψ_{RLT} to OPT-RLT, we have $0 \leq \hat{\eta}_{\text{vac}} \leq \eta_{\text{vac}}$. To show that $\eta_{\text{vac}}^* - \eta_{\text{vac}} \leq \frac{|Q|}{L}$, it is sufficient to show that $\eta_{\text{vac}}^* - \hat{\eta}_{\text{vac}} \leq \frac{|Q|}{L}$ for some feasible solution $\hat{\psi}_{\text{RLT}}$. In the following proof, we will construct such a feasible solution $\hat{\psi}_{\text{RLT}}$ to problem OPT-RLT so that $\eta_{\text{vac}}^* - \hat{\eta}_{\text{vac}} \leq \frac{|Q|}{L}$.

Recall that an optimal (unknown) solution ψ^* to problem OPT consists of $(f_{ij}^*, f_{iB}^*, p_i^*, \eta_{\text{vac}}^*, \eta_k^*)$. For a given L , we construct a solution $\hat{\psi}_{\text{RLT}} = (f_{ij}, f_{iB}, \hat{p}_i, \hat{\eta}_{\text{vac}}, \hat{z}_{kl}, \hat{\gamma}_{ikl})$ for problem OPT-RLT based on $\psi^* = (f_{ij}^*, f_{iB}^*, p_i^*, \eta_{\text{vac}}^*, \eta_k^*)$ as follows. We let $\hat{f}_{ij} = f_{ij}^*$, $\hat{f}_{iB} = f_{iB}^*$, and $\hat{p}_i = p_i^*$. Then, for the rest of the solution $\hat{\psi}_{\text{RLT}}$ (i.e., $\hat{\eta}_{\text{vac}}$, \hat{z}_{kl} , and $\hat{\gamma}_{ikl}$), we do the following. First, we round ‘‘up’’ η_k^* to the nearest discrete point $\eta_{k\xi} = \frac{\xi}{L}$, where $\xi = \lceil \eta_k^* \cdot L \rceil$. The rounding error for each $k \in Q$ is

$$\eta_{k\xi} - \eta_k^* \leq \frac{1}{L}. \quad (23)$$

For \hat{z}_{kl} , we set $\hat{z}_{k\xi} = 1$ and $\hat{z}_{kl} = 0$, for $l = 0, \dots, L, l \neq \xi$. Then, for $\hat{\gamma}_{ikl}$, we set $\hat{\gamma}_{ikl} = \hat{z}_{kl} \cdot \hat{p}_i$, for $i \in \mathcal{N}_k, k \in Q, l = 0, 1, \dots, L$. Finally, for $\hat{\eta}_{\text{vac}}$, based on (22), we set it to

$$\hat{\eta}_{\text{vac}} = \min_{i \in \mathcal{N}_k, k \in Q} \left\{ 1 - \sum_{j \in Q} \sum_{l=0}^L \eta_{jl} \cdot \hat{z}_{jl} - \frac{\tau_{\text{TSP}}}{E_{\text{max}} - E_{\text{min}}} \cdot \left(\hat{p}_i - \sum_{l=0}^L \eta_{kl} \cdot \hat{\gamma}_{ikl} \right) \right\}. \quad (24)$$

Now we prove that the above newly constructed $\hat{\psi}_{\text{RLT}} = (\hat{f}_{ij}, \hat{f}_{iB}, \hat{p}_i, \hat{\eta}_{\text{vac}}, \hat{z}_{kl}, \hat{\gamma}_{ikl})$ is indeed a feasible solution to problem OPT-RLT. That is, we will show that $\hat{\psi}_{\text{RLT}}$ satisfies constraints (2), (3), (16), (18), and (20)–(22). Since ψ^* is an optimal solution to problem OPT, ψ^* satisfies (2), (3), (10), and (11). Since $\hat{f}_{ij} = f_{ij}^*$, $\hat{f}_{iB} = f_{iB}^*$, and $\hat{p}_i = p_i^*$, $\hat{\psi}_{\text{RLT}}$ also satisfies (2) and (3). From the construction of \hat{z}_{kl} and $\hat{\gamma}_{ikl}$, we know that $\hat{\psi}_{\text{RLT}}$ satisfies constraints (16) and (20). Now we consider (18). We have $\hat{p}_i - U_i \sum_{l=0}^L \eta_{kl} \cdot \hat{z}_{kl} \leq p_i^* - U_i \cdot \eta_k^* \leq 0$, where the first inequality holds due to $\hat{p}_i = p_i^*$ and $\sum_{l=0}^L \eta_{kl} \cdot \hat{z}_{kl} = \eta_{k\xi} \geq \eta_k^*$ (because $\hat{z}_{k\xi} = 1$ and $\hat{z}_{kl} = 0, l = 0, 1, \dots, L, l \neq \xi$), and the second inequality holds since ψ^* satisfies (11). To verify constraint (21), we multiply $0 \leq \hat{p}_i \leq U_i$ by \hat{z}_{kl} , and have $0 \leq \hat{z}_{kl} \cdot \hat{p}_i \leq U_i \cdot \hat{z}_{kl}$, or equivalently, $0 \leq \hat{\gamma}_{ikl} \leq U_i \cdot \hat{z}_{kl}$. Constraint (22) can be verified directly from (24). Thus, the newly constructed solution $\hat{\psi}_{\text{RLT}}$ is indeed a feasible solution to problem OPT-RLT.

Now we show that $\eta_{\text{vac}}^* - \hat{\eta}_{\text{vac}} \leq \frac{|Q|}{L}$. Since ψ^* is an optimal solution to problem OPT, constraint (10) must be binding for some $i \in \mathcal{N}$ under ψ^* . That is

$$\eta_{\text{vac}}^* = \min_{i \in \mathcal{N}_k, k \in Q} \left\{ 1 - \sum_{j \in Q} \eta_j^* - \frac{\tau_{\text{TSP}}}{E_{\text{max}} - E_{\text{min}}} (1 - \eta_k^*) \cdot p_i^* \right\}. \quad (25)$$

We have

$$\begin{aligned} \eta_{\text{vac}}^* - \hat{\eta}_{\text{vac}} &= \min_{i \in \mathcal{N}_k, k \in Q} \left\{ 1 - \sum_{j \in Q} \eta_j^* - \frac{\tau_{\text{TSP}}}{E_{\text{max}} - E_{\text{min}}} (1 - \eta_k^*) \cdot p_i^* \right\} \\ &\quad - \min_{i \in \mathcal{N}_k, k \in Q} \left\{ 1 - \sum_{j \in Q} \sum_{l=0}^L \eta_{jl} \cdot \hat{z}_{jl} - \frac{\tau_{\text{TSP}}}{E_{\text{max}} - E_{\text{min}}} \cdot \left(\hat{p}_i - \sum_{l=0}^L \eta_{kl} \cdot \hat{\gamma}_{ikl} \right) \right\} \\ &= \left(\sum_{j \in Q} \sum_{l=0}^L \eta_{jl} \cdot \hat{z}_{jl} - \sum_{j \in Q} \eta_j^* \right) \\ &\quad - \frac{\tau_{\text{TSP}}}{E_{\text{max}} - E_{\text{min}}} \cdot \max_{i \in \mathcal{N}_k, k \in Q} \left\{ (1 - \eta_k^*) \cdot p_i^* \right\} \\ &\quad + \frac{\tau_{\text{TSP}}}{E_{\text{max}} - E_{\text{min}}} \cdot \max_{i \in \mathcal{N}_k, k \in Q} \left\{ \hat{p}_i - \sum_{l=0}^L \eta_{kl} \cdot \hat{\gamma}_{ikl} \right\} \\ &= \left(\sum_{j \in Q} \eta_{j\xi} - \sum_{j \in Q} \eta_j^* \right) \\ &\quad - \frac{\tau_{\text{TSP}}}{E_{\text{max}} - E_{\text{min}}} \cdot \max_{i \in \mathcal{N}_k, k \in Q} \left\{ (1 - \eta_k^*) \cdot p_i^* \right\} \\ &\quad + \frac{\tau_{\text{TSP}}}{E_{\text{max}} - E_{\text{min}}} \cdot \max_{i \in \mathcal{N}_k, k \in Q} \left\{ \hat{p}_i - \sum_{l=0}^L \eta_{kl} \cdot \hat{z}_{kl} \cdot \hat{p}_i \right\} \\ &= \sum_{j \in Q} (\eta_{j\xi} - \eta_j^*) \end{aligned}$$

$$\begin{aligned}
& - \frac{\tau_{\text{TSP}}}{E_{\max} - E_{\min}} \cdot \max_{i \in \mathcal{N}_k, k \in \mathcal{Q}} \{(1 - \eta_k^*) \cdot p_i^*\} \\
& + \frac{\tau_{\text{TSP}}}{E_{\max} - E_{\min}} \cdot \max_{i \in \mathcal{N}_k, k \in \mathcal{Q}} \{(1 - \eta_{k\xi}) \cdot p_i^*\} \\
& \leq \sum_{j \in \mathcal{Q}} (\eta_{j\xi} - \eta_j^*) \leq \frac{|\mathcal{Q}|}{L}
\end{aligned}$$

where the first equality holds by (25) and (24), the third equality holds due to $\sum_{l=0}^L \eta_{jl} \cdot \hat{z}_{jl} = \eta_{j\xi}$ (since only $\hat{z}_{j\xi} = 1$ and $\hat{z}_{jl} = 0$, $l = 0, 1, \dots, L$, $l \neq \xi$) and $\hat{\gamma}_{ikl} = \hat{z}_{kl} \cdot \hat{p}_i$, the fourth equality holds due to $\hat{p}_i = p_i^*$ and $\sum_{l=0}^L \eta_{kl} \cdot \hat{z}_{kl} = \eta_{k\xi}$, the sixth inequality holds due to $\eta_{k\xi} \geq \eta_k^*$ for $k \in \mathcal{Q}$, and the last inequality holds by (23). This completes the proof. ■

Performance Guarantee: Lemma 4 gives an upper bound of the performance gap between η_{vac} and η_{vac}^* for a given L . The following lemma shows how to choose L so that this performance gap is no more than ϵ ($0 < \epsilon \ll 1$).

Lemma 5: For a given ϵ , $0 < \epsilon \ll 1$, if $L = \lceil \frac{|\mathcal{Q}|}{\epsilon} \rceil$, we have $\eta_{\text{vac}}^* - \eta_{\text{vac}} \leq \epsilon$.

Proof: By Lemma 4, we know $\eta_{\text{vac}}^* - \eta_{\text{vac}} \leq \frac{|\mathcal{Q}|}{L}$. To have $\eta_{\text{vac}}^* - \eta_{\text{vac}} \leq \epsilon$, it is sufficient to have $\frac{|\mathcal{Q}|}{L} \leq \epsilon$, or $L = \lceil \frac{|\mathcal{Q}|}{\epsilon} \rceil$. This completes the proof. ■

VII. NUMERICAL RESULTS

In this section, we present some numerical results to demonstrate our proposed solution. We also demonstrate how our solution can address the scalability issue when the density of sensor nodes increases.

A. Simulation Settings

We assume sensor nodes are deployed over a $1000 \times 1000\text{-m}^2$ area. The number of nodes in the network will be specified for each instance in the study. The base station is at (500, 500) (in meters), and the WCV's home service station is assumed to be at the origin. The traveling speed of the WCV is $V = 5$ m/s. The data rate R_i , $i \in \mathcal{N}$, from each node is randomly generated within [1,10] kb/s. The power consumption coefficients are $\beta_1 = 50$ nJ/b, $\beta_2 = 0.0013$ pJ/(b · m⁴), and $\rho = 50$ nJ/b [25]. The path-loss index is $\alpha = 4$.

For the battery at a sensor node, we choose a regular NiMH battery, and its nominal cell voltage and electricity volume is 1.2 V/2.5 Ah. We have $E_{\max} = 1.2 \text{ V} \times 2.5 \text{ A} \times 3600 \text{ s} = 10.8 \text{ kJ}$ [14]. We let $E_{\min} = 0.05 \cdot E_{\max} = 540 \text{ J}$. For $\mu(D_i)$, we refer to the experimental data on wireless energy transfer efficiency in [13]. Through curve fitting to [13, Fig. 3], we obtain $\mu(D_i) = -0.0958D_i^2 - 0.0377D_i + 1.0$. Assuming $U_{\text{Full}} = 5 \text{ W}$ and $\delta = 1 \text{ W}$, we have $D = 2.7 \text{ m}$ for a cell's side length. We set $\epsilon = 0.1$ for the numerical results.

B. Results for a 100-Node Network

We first present complete results for a 100-node network. Table II gives the location of each node and its data rate for the 100-node network. These 100 nodes are distributed in $|\mathcal{Q}| = 32$ selected cells, and Table III gives the location of each cell as well as the number of sensor nodes it contains. The shortest Hamiltonian cycle that threads all cells $k \in \mathcal{Q}$ and the service station is found by the Concorde TSP solver [4], which

TABLE II
LOCATION AND DATA RATE R_i FOR EACH NODE IN A 100-NODE NETWORK

Node index	Location (m)	R_i (kb/s)	Node index	Location (m)	R_i (kb/s)
1	(140.8,905.4)	3	51	(613.9,474.1)	9
2	(977.8,913.0)	5	52	(837.1,6.1)	2
3	(679.9,92.7)	4	53	(635.8,216.4)	4
4	(325.8,378.1)	5	54	(165.7,109.6)	7
5	(196.2,526.8)	8	55	(634.9,218.4)	1
6	(546.5,967.0)	2	56	(747.2,33.2)	7
7	(323.4,329.4)	7	57	(821.4,608.6)	5
8	(747.7,33.4)	3	58	(250.1,839.1)	10
9	(838.3,678.0)	1	59	(990.6,617.0)	6
10	(692.5,461.4)	9	60	(977.9,909.0)	4
11	(918.4,517.9)	1	61	(585.6,623.4)	5
12	(613.6,476.1)	1	62	(678.6,91.7)	1
13	(586.2,621.8)	4	63	(613.5,475.9)	1
14	(440.2,17.7)	4	64	(438.8,17.3)	2
15	(813.3,749.9)	7	65	(836.5,680.4)	10
16	(886.2,612.7)	7	66	(321.9,331.2)	3
17	(804.9,329.4)	5	67	(752.3,714.6)	9
18	(633.7,218.4)	4	68	(679.6,93.7)	8
19	(753.3,713.0)	9	69	(838.0,677.4)	6
20	(163.7,108.6)	2	70	(897.2,709.2)	2
21	(672.0,318.1)	10	71	(750.8,712.4)	3
22	(250.2,840.1)	1	72	(635.5,217.4)	7
23	(732.3,965.0)	4	73	(585.4,622.0)	6
24	(197.4,672.2)	6	74	(732.0,966.2)	3
25	(92.7,967.7)	1	75	(91.5,971.3)	2
26	(990.1,617.4)	4	76	(918.6,514.1)	2
27	(804.3,352.0)	7	77	(166.0,109.0)	8
28	(821.5,609.8)	7	78	(90.6,967.7)	10
29	(898.3,708.4)	6	79	(813.4,749.7)	1
30	(688.4,59.1)	3	80	(686.9,59.7)	10
31	(837.3,4.5)	2	81	(587.1,622.4)	2
32	(451.2,135.5)	1	82	(838.2,680.4)	4
33	(979.3,911.8)	8	83	(249.7,842.5)	3
34	(678.9,93.3)	8	84	(139.9,902.0)	7
35	(751.6,714.2)	6	85	(691.4,459.4)	3
36	(633.8,217.0)	9	86	(747.3,36.0)	5
37	(452.9,133.7)	3	87	(803.9,327.0)	7
38	(633.6,217.8)	1	88	(164.6,108.4)	3
39	(884.4,613.9)	1	89	(197.8,670.4)	5
40	(197.1,523.2)	6	90	(820.8,610.2)	3
41	(813.8,747.7)	5	91	(140.8,904.6)	9
42	(804.1,326.6)	4	92	(546.3,965.4)	4
43	(732.9,966.2)	3	93	(886.8,613.1)	8
44	(690.1,460.2)	7	94	(671.5,318.9)	8
45	(669.9,319.1)	7	95	(248.7,842.9)	4
46	(195.9,670.2)	10	96	(670.6,318.1)	7
47	(440.7,17.1)	2	97	(613.3,477.1)	9
48	(670.2,319.3)	10	98	(614.2,475.7)	5
49	(585.1,624.2)	1	99	(452.2,133.1)	7
50	(896.5,708.4)	8	100	(197.4,670.6)	4

is shown in Fig. 9. For this optimal cycle, $D_{\text{TSP}} = 5110 \text{ m}$ and $\tau_{\text{TSP}} = 1022 \text{ s} \approx 0.28 \text{ h}$. For the target performance gap $\epsilon = 0.1$, we have cycle time $\tau = 13.95 \text{ h}$, vacation time $\tau_{\text{vac}} = 10.26 \text{ h}$, total charging time $13.95 - 10.26 - 0.28 = 3.41 \text{ h}$, and the objective $\eta_{\text{vac}} = 73.55\%$.

Due to the large number of sensor nodes (i.e., 100) and the potential large number of different outgoing subflows from each sensor node (up to 100), it will take too much space to show these subflows in the network (up to 10000). For illustration, we show flow routing (and rates) at nodes 1 and 4:

- 1) At node 1: Self-generated rate $R_1 = 3.0$, outgoing flow rates $f_{1,92} = 0.3$, $f_{1,95} = 2.7$, all in kb/s;
- 2) At node 4: Self-generated rate $R_4 = 5.0$, incoming flow rates $f_{5,4} = 24.5$, $f_{39,4} = 21.5$, outgoing flow rates $f_{4,7} = 13.7$, $f_{4,66} = 37.3$, all in kb/s.

Corollary 1.1 says that each sensor node in the network is fully charged to E_{\max} when the WCV departs its cell, which is

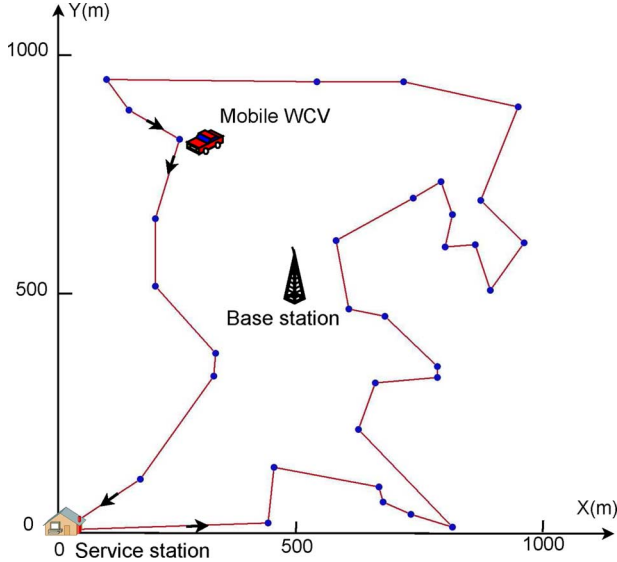


Fig. 9. Optimal traveling path (assuming counterclockwise direction) for the 100-node sensor network. The 100 nodes are distributed in 32 cells, with the center of each cell being represented as a point in the figure.

TABLE III
CELLS INDEX, LOCATION OF CELL CENTER, SENSOR NODES IN EACH CELL,
CELL TRAVELING ORDER ALONG THE PATH, AND CHARGING TIME
AT EACH CELL FOR THE 100-NODE NETWORK

Cell index	Location of cell center (m)	Sensor nodes in the cell	Travel order	τ_k (s)
1	(140.4, 904.1)	1, 84, 91	26	157
2	(452.3, 134.8)	32, 37, 99	2	314
3	(837.0, 6.2)	31, 52	6	157
4	(687.1, 60.0)	30, 80	4	157
5	(897.8, 710.1)	29, 50, 70	21	157
6	(820.8, 609.5)	28, 57, 90	17	628
7	(804.6, 352.3)	27	10	157
8	(990.9, 618.9)	26, 59	20	157
9	(91.8, 969.6)	25, 75, 78	25	157
10	(197.1, 670.3)	24, 46, 89, 100	28	2510
11	(731.7, 964.9)	23, 43, 74	23	314
12	(249.8, 841.0)	22, 58, 83, 95	27	471
13	(670.9, 317.2)	21, 45, 48, 94, 96	8	314
14	(164.7, 109.1)	20, 54, 77, 88	32	471
15	(751.9, 714.7)	19, 35, 67, 71	14	314
16	(634.5, 216.7)	18, 36, 38, 53, 55, 72	7	157
17	(804.6, 328.9)	17, 42, 87	9	157
18	(885.6, 614.2)	16, 39, 93	18	157
19	(812.7, 749.8)	15, 41, 79	15	157
20	(440.1, 15.6)	14, 47, 64	1	157
21	(585.9, 623.5)	13, 49, 61, 73, 81	13	157
22	(614.3, 476.2)	12, 51, 63, 97, 98	12	314
23	(918.0, 516.0)	11, 76	19	157
24	(691.2, 459.9)	10, 44, 85	11	157
25	(837.0, 679.7)	9, 65, 69, 82	16	157
26	(747.9, 34.3)	8, 56, 86	5	157
27	(322.6, 331.3)	7, 66	31	2353
28	(545.4, 964.9)	6, 92	24	157
29	(197.1, 525.3)	5, 40	29	784
30	(326.7, 380.4)	4	30	157
31	(679.0, 92.8)	3, 34, 62, 68	3	157
32	(978.8, 911.1)	2, 33, 60	22	314

confirmed by our numerical results. By Property 3, we find that in an optimal solution, there exists at least one equilibrium node in each cell $k \in \mathcal{Q}$. In our numerical results, all 32 cells contain equilibrium nodes.

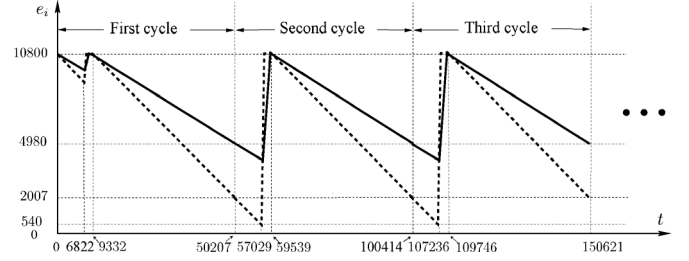


Fig. 10. Energy cycle behavior of an equilibrium node (node 24, in solid curve) and a nonequilibrium node (node 89, in dashed curve) in the 100-node network. Node 89 is also a bottleneck node.

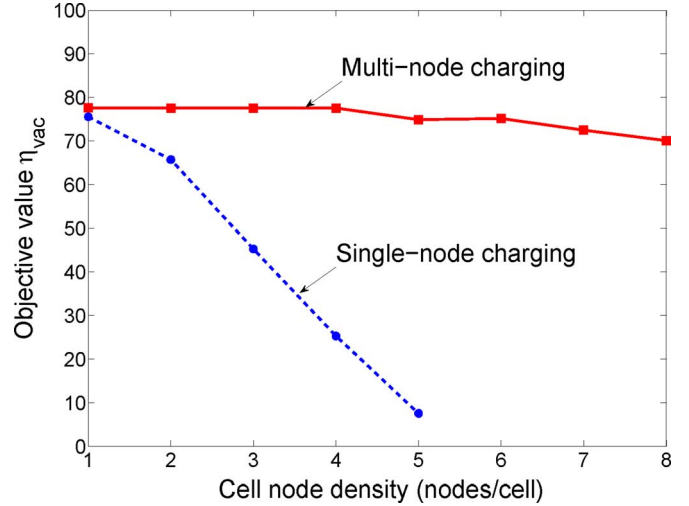


Fig. 11. Achievable objective value as a function of node density under multi-node and single-node charging technologies.

To examine energy behavior at sensor nodes, consider sensor nodes in cell 10. There are four sensor nodes in this cell, nodes 24 and 46 are equilibrium nodes, while nodes 89 and 100 are not. Fig. 10 shows the energy behavior of node 24 (solid curve) and node 89 (dashed curve). Note that node 24 does not have any saturation period except in the initial first cycle, while node 89 has saturation period in every cycle.

By Property 2, we find that there exists an energy bottleneck node in the network with its energy dropping to E_{\min} during a cycle. This property is also confirmed in our numerical results. This bottleneck node is the 89th node, whose energy behavior is shown in Fig. 10.

C. Scalability Comparison

In this section, we demonstrate how multi-node charging can address the scalability problem in wireless energy transfer. We consider $|\mathcal{Q}| = 25$ cells and increase node density in these cells from 1 to 8 per cell. For each density, we compare multi-node charging with single-node charging. Fig. 11 shows the numerical results. We have two observations.

- 1) The achievable objective value under multi-node charging remains steady when node density increases from 1 to 8, with only slight decrease. On the other hand, the achievable objective value under single-node charging drops very quickly when node density increases, and a feasible solution does not exist when node density is beyond 5.

TABLE IV
DETAILS OF COMPARISON BETWEEN MULTI-NODE CHARGING AND
SINGLE-NODE CHARGING

Density (Nodes /Cell)	Multi-node Charging			Single-node Charging		
	τ (h)	$\sum_{k \in \mathcal{Q}} \tau_k$ (h)	η_{vac}	τ (h)	$\sum_{k \in \mathcal{Q}} \tau_k$ (h)	η_{vac}
1	8.28	1.59	77.59%	8.12	1.84	75.58%
2	8.27	1.59	77.58%	4.72	1.46	65.75%
3	8.22	1.58	77.57%	7.32	3.86	45.24%
4	8.24	1.58	77.57%	5.64	4.06	25.29%
5	7.21	1.76	74.91%	6.20	5.58	7.54%
6	8.28	1.79	75.19%	-	-	-
7	7.33	1.75	72.50%	-	-	-
8	6.83	1.77	70.11%	-	-	-

2) Over the entire density range (from 1 to 8), the objective value under multi-node charging is always higher than that under single-node charging, and the gap between them widens as density increases.

Table IV gives more details for the study shown in Fig. 11. Note that under multi-node charging, the achievable objective value at density 6 is slightly larger than that at density 5. This local fluctuation is due to more possibilities for routing when density increases. However, this is only a local fluctuation. The prevailing trend is that η_{vac} decreases as density increases.

VIII. CONCLUSION

In this paper, we exploited recent advances in multi-node wireless energy transfer technology to charge the batteries of sensor nodes in a WSN. Our approach was to develop a formal optimization framework by jointly optimizing traveling path, flow routing, and charging time at each cell. By employing discretization and a novel reformulation-linearization technique, we developed a provably near-optimal solution for any desired level of accuracy. Using numerical results, we demonstrated the advantage of multi-node wireless energy transfer technology and showed how it addressed the charging scalability problem in a dense wireless sensor network.

APPENDIX

Proof of Lemma 1: The “only if” part of the lemma [i.e., (6) and (7) are necessary conditions] was already proved in the discussion in Section III-D. We now prove the “if” part of the lemma, i.e., if (6) and (7) hold, then $e_i(t) \geq E_{\min}$ for all $t \geq 0$, $i \in \mathcal{N}$.

Recall that, to have $e_i(t) \geq E_{\min}$, $i \in \mathcal{N}$, it is sufficient to have $e_i(m\tau + a_k) \geq E_{\min}$, for $m \in \mathbb{N}$, $i \in \mathcal{N}$. We consider $e_i(a_k)$ and $e_i(m\tau + a_k)$ for $m \geq 1$, respectively. The first cycle (i.e., $m = 0$) is solely considered since it starts with E_{\max} , and the succeeding cycle (i.e., $m \geq 1$) starts with a nonfull energy level. Note that for all cycles, the traveling path P , time intervals τ , τ_P , τ_{vac} , and τ_k , the flow rates f_{ij} and f_{iB} , and power consumption p_i are identical.

When $m = 0$, we show that $e_i(a_k) \geq E_{\min}$. We see that

$$\begin{aligned} e_i(a_k) &= e_i(0) - p_i \cdot a_k = E_{\max} - p_i \cdot a_k \\ &> E_{\max} - p_i \cdot (\tau - \tau_k) \geq E_{\min}, \quad i \in \mathcal{N} \end{aligned}$$

where the second equality holds due to $e_i(0) = E_{\max}$, the third inequality holds due to $a_k + \tau_k < \tau$, and the last inequality holds

due to (6). That is, each sensor has sufficient energy to support itself until the WCV’s first arrival.

Now we show $e_i(m\tau + a_k) \geq 1$. It is sufficient to show $e_i(\tau + a_k) \geq E_{\min}$ and $e_i(2\tau) = e_i(\tau)$. It follows that $e_i(m\tau + a_k) \geq E_{\min}$ for all $m \geq 1$ due to periodicity.

To show $e_i(\tau + a_k) \geq E_{\min}$, we have

$$\begin{aligned} e_i(\tau + a_k) &= e_i(a_k + \tau_k) - [(\tau + a_k) - (a_k + \tau_k)] \cdot p_i \\ &= e_i(a_k + \tau_k) - (\tau - \tau_k) \cdot p_i \end{aligned}$$

where $e_i(a_k + \tau_k) = \min\{e_i(a_k) + (U_i - p_i) \cdot \tau_k, E_{\max}\}$ considering that node $i \in \mathcal{N}_k$ may be under saturation state during $[a_k, a_k + \tau_k]$. We find that

$$\begin{aligned} e_i(a_k) + (U_i - p_i) \cdot \tau_k &= e_i(0) - a_k \cdot p_i + (U_i - p_i) \cdot \tau_k \\ &= E_{\max} - (a_k + \tau_k) \cdot p_i + U_i \cdot \tau_k \\ &> E_{\max} - \tau \cdot p_i + U_i \cdot \tau_k \\ &\geq E_{\max} \end{aligned}$$

where the second equality holds due to $e_i(0) = E_{\max}$, the third inequality holds due to $a_k + \tau_k < \tau$, and the last inequality holds due to (7). We then have

$$e_i(a_k + \tau_k) = E_{\max} \quad (26)$$

Therefore

$$\begin{aligned} e_i(\tau + a_k) &= e_i(a_k + \tau_k) - (\tau - \tau_k) \cdot p_i \\ &= E_{\max} - (\tau - \tau_k) \cdot p_i \\ &\geq E_{\min} \end{aligned} \quad (27)$$

where the last inequality holds by (6).

We also show that $e_i(2\tau) = e_i(\tau)$. We find that

$$\begin{aligned} e_i(\tau) &= e_i(a_k + \tau_k) - (\tau - a_k - \tau_k) \cdot p_i \\ &= E_{\max} - (\tau - a_k - \tau_k) \cdot p_i \end{aligned} \quad (28)$$

where the second equality holds by (26). We also have

$$\begin{aligned} e_i(2\tau) &= e_i(\tau + a_k + \tau_k) - [2\tau - (\tau + a_k + \tau_k)] \cdot p_i \\ &= e_i(\tau + a_k + \tau_k) - (\tau - a_k - \tau_k) \cdot p_i \end{aligned}$$

where $e_i(\tau + a_k + \tau_k) = \min\{e_i(\tau + a_k) + (U_i - p_i) \cdot \tau_k, E_{\max}\}$. It follows that

$$\begin{aligned} e_i(\tau + a_k) + (U_i - p_i) \cdot \tau_k &= E_{\max} - (\tau - \tau_k) \cdot p_i + (U_i - p_i) \cdot \tau_k \\ &= E_{\max} - \tau \cdot p_i + U_i \cdot \tau_k \\ &\geq E_{\max} \end{aligned}$$

where the first equality holds by (27), and the last inequality holds due to (7). We then have

$$e_i(\tau + a_k + \tau_k) = E_{\max} \quad (29)$$

and it follows that

$$\begin{aligned} e_i(2\tau) &= e_i(\tau + a_k + \tau_k) - (\tau - a_k - \tau_k) \cdot p_i \\ &= E_{\max} - (\tau - a_k - \tau_k) \cdot p_i \\ &= e_i(\tau) \end{aligned}$$

where the second equality holds by (29), and the last equality holds by (28).

Therefore, if both constraints (6) and (7) are satisfied, $e_i(t) \geq E_{\min}$ for all $t \geq 0$, $i \in \mathcal{N}$. ■

Proof of Property 2: The proof is based on contradiction. Suppose there exists an optimal solution $\varphi^* = (\tau^*, \tau_{\text{vac}}^*, \tau_k^*, f_{ij}^*, f_{iB}^*, p_i^*)$, where none of the nodes in the network have their energy level ever drop to E_{\min} , i.e., $e_i^*(\tau^* + a_k^*) > E_{\min}$ for all $i \in \mathcal{N}$. Then, we can construct a new solution $\hat{\varphi} = (\hat{\tau}, \hat{\tau}_{\text{vac}}, \hat{\tau}_k, \hat{f}_{ij}, \hat{f}_{iB}, \hat{p}_i)$ by choosing $\gamma = \min_{i \in \mathcal{N}_k, k \in \mathcal{Q}} \left\{ \frac{E_{\max} - E_{\min}}{(\tau^* - \tau_k^*) p_i^*} \right\} - 1$ and letting $\hat{\tau} = (1 + \gamma)\tau^*$, $\hat{\tau}_k = (1 + \gamma)\tau_k^*$, $\hat{\tau}_{\text{vac}} = \tau_{\text{vac}}^* + \gamma(\tau^* - \sum_{k \in \mathcal{Q}} \tau_k^*)$, $\hat{f}_{ij} = f_{ij}^*$, $\hat{f}_{iB} = f_{iB}^*$, and $\hat{p}_i = p_i^*$.

Now we show $\gamma > 0$. Since $e_i^*(\tau^* + a_k^*) > E_{\min}$ for all $i \in \mathcal{N}$, we have $e_i^*(\tau^* + a_k^*) = E_{\max} - (\tau^* - \tau_k^*) p_i^* > E_{\min}$ for all $i \in \mathcal{N}$, i.e., $\min_{i \in \mathcal{N}_k, k \in \mathcal{Q}} \{E_{\max} - (\tau^* - \tau_k^*) p_i^*\} > E_{\min}$. It follows $E_{\max} - \max_{i \in \mathcal{N}_k, k \in \mathcal{Q}} \{(\tau^* - \tau_k^*) p_i^*\} > E_{\min}$, or $\frac{E_{\max} - E_{\min}}{\max_{i \in \mathcal{N}_k, k \in \mathcal{Q}} \{(\tau^* - \tau_k^*) p_i^*\}} > 1$. Thus, $\gamma = \min_{i \in \mathcal{N}_k, k \in \mathcal{Q}} \left\{ \frac{E_{\max} - E_{\min}}{(\tau^* - \tau_k^*) p_i^*} \right\} - 1 = \frac{E_{\max} - E_{\min}}{\max_{i \in \mathcal{N}_k, k \in \mathcal{Q}} \{(\tau^* - \tau_k^*) p_i^*\}} - 1 > 0$.

The feasibility of $\hat{\varphi}$ can be verified similarly as that in the proof of Property 3. We now show that this new feasible solution $\hat{\varphi}$ can offer a better (increased) objective value. By (8), we have $\frac{\hat{\tau}_{\text{vac}}}{\hat{\tau}} = 1 - \frac{\hat{\tau}_p}{\hat{\tau}} - \frac{\sum_{k \in \mathcal{Q}} \hat{\tau}_k}{\hat{\tau}}$. Since $\hat{\tau} = (1 + \gamma)\tau^*$, $\hat{\tau}_k = (1 + \gamma)\tau_k^*$, $\hat{\tau}_p = \tau_p^*$, it follows that $\frac{\hat{\tau}_{\text{vac}}}{\hat{\tau}} = 1 - \frac{\tau_p^*}{(1 + \gamma)\tau^*} - \frac{\sum_{k \in \mathcal{Q}} (1 + \gamma)\tau_k^*}{(1 + \gamma)\tau^*} > 1 - \frac{\tau_p^*}{\tau^*} - \frac{\sum_{k \in \mathcal{Q}} \tau_k^*}{\tau^*} = \frac{\tau_{\text{vac}}^*}{\tau^*}$, i.e., $\frac{\hat{\tau}_{\text{vac}}}{\hat{\tau}} > \frac{\tau_{\text{vac}}^*}{\tau^*}$. This contradicts the assumption that φ^* is an optimal solution. The proof is complete. ■

Proof of Property 3: The proof is based on contradiction. Suppose there exists an optimal solution $\varphi = (f_{ij}, f_{iB}, p_i, \eta_{\text{vac}}, \eta_k)$ to problem OPT, where there is no equilibrium node in some cell $k \in \mathcal{Q}$, i.e., $p_i - U_i \cdot \eta_k < 0$ for all $i \in \mathcal{N}_k$. Let $\mathcal{Q}_{\text{nb}} = \{k | p_i - U_i \cdot \eta_k < 0, i \in \mathcal{N}_k\}$ be the set of these cells. We show how to construct a new solution $\hat{\varphi}$ with a better objective value, thus leading to contradiction. Define $\hat{\varphi} = (\hat{f}_{ij}, \hat{f}_{iB}, \hat{p}_i, \hat{\eta}_{\text{vac}}, \hat{\eta}_k)$ by letting

$$\hat{f}_{ij} = f_{ij} \quad \hat{f}_{iB} = f_{iB} \quad \hat{p}_i = p_i \quad (30)$$

$$\hat{\eta}_k = \begin{cases} \eta_k, & \text{if } k \notin \mathcal{Q}_{\text{nb}} \\ \frac{\max_{i \in \mathcal{N}_k} \{p_i\}}{U_i}, & \text{if } k \in \mathcal{Q}_{\text{nb}} \end{cases} \quad (31)$$

$$\hat{\eta}_{\text{vac}} = \min_{i \in \mathcal{N}_k, k \in \mathcal{Q}} \left\{ 1 - \sum_{j \in \mathcal{Q}} \hat{\eta}_j - \frac{\tau_{\text{TSP}}}{E_{\max} - E_{\min}} (1 - \hat{\eta}_k) \cdot \hat{p}_i \right\}. \quad (32)$$

Now we show that $\hat{\varphi}$ is feasible to problem OPT. By feasibility, we mean that it meets the flow conservation constraint (2) and the energy constraints (3), (10), and (11). Since φ

is a feasible solution, it satisfies (2), (3), (10), and (11). By (30), $\hat{\varphi}$ also satisfies constraints (2) and (3). Constraints (10) can be verified directly from (32). Now we consider constraint (11), which can be easily verified for $k \notin \mathcal{Q}_{\text{nb}}$ due to $\hat{p}_i = p_i$ and (31). For $k \in \mathcal{Q}_{\text{nb}}$, $\hat{p}_i - U_i \cdot \hat{\eta}_k = p_i - \max_{j \in \mathcal{N}_k} \{p_j\} \leq 0$, where the equality holds due to $\hat{p}_i = p_i$ and (31). Therefore, $\hat{\varphi}$ is feasible to problem OPT.

We now show that this new feasible solution $\hat{\varphi}$ can offer a better (increased) objective value, i.e., $\hat{\eta}_{\text{vac}} > \eta_{\text{vac}}$. Let $g(\eta_1, \eta_2, \dots, \eta_{|\mathcal{Q}|}) = 1 - \sum_{j \in \mathcal{Q}} \eta_j - \frac{\tau_{\text{TSP}}}{E_{\max} - E_{\min}} \cdot \max_{i \in \mathcal{N}_k, k \in \mathcal{Q}} \{(1 - \eta_k) \cdot p_i\}$, and assume that $q \in \mathcal{Q}$ is a particular cell such that $(1 - \eta_q) \cdot \max_{i \in \mathcal{N}_q} \{p_i\} = \max_{i \in \mathcal{N}_k, k \in \mathcal{Q}} \{(1 - \eta_k) \cdot p_i\}$. Then, we have

$$\frac{\partial g(\cdot)}{\partial \eta_k} = \begin{cases} -1 + \frac{\tau_{\text{TSP}}}{E_{\max} - E_{\min}} \cdot \max_{i \in \mathcal{N}_q} \{p_i\}, & \text{if } k = q \\ -1, & \text{otherwise.} \end{cases}$$

We show $g(\cdot)$ is a decreasing function of variables η_k for $k \in \mathcal{Q}$. It is sufficient to show that $\frac{\partial g(\cdot)}{\partial \eta_k} < 0$ for $k \in \mathcal{Q}$. Clearly, we only need to consider the case of $k = q$. We see $\tau_{\text{TSP}} \cdot p_i < (\tau - \tau_k) \cdot p_i \leq E_{\max} - E_{\min}$, $i \in \mathcal{N}$, where the first inequality holds due to $\tau_{\text{TSP}} + \tau_k < \tau$, and the second inequality due to (6) [which is a reformulation reversely from (10)]. We have $\frac{\tau_{\text{TSP}}}{E_{\max} - E_{\min}} \cdot \max_{i \in \mathcal{N}_q} \{p_i\} < 1$, or $\frac{\partial g(\cdot)}{\partial \eta_k} < 0$ for the case of $k = q$.

Now we are ready to show $\hat{\eta}_{\text{vac}} > \eta_{\text{vac}}$. For $k \in \mathcal{Q}_{\text{nb}}$, we have $\hat{\eta}_k = \frac{\max_{i \in \mathcal{N}_k} \{p_i\}}{U_i} < \eta_k$, where the equality holds by (31) and the inequality holds by the definition of \mathcal{Q}_{nb} . By (31), $\hat{\eta}_k = \eta_k$ for $k \notin \mathcal{Q}_{\text{nb}}$. Since $g(\cdot)$ is a decreasing function of variables η_k and $\mathcal{Q}_{\text{nb}} \neq \emptyset$, we have $g(\hat{\eta}_1, \hat{\eta}_2, \dots, \hat{\eta}_{|\mathcal{Q}|}) > g(\eta_1, \eta_2, \dots, \eta_{|\mathcal{Q}|})$. Therefore, $\hat{\eta}_{\text{vac}} = g(\hat{\eta}_1, \hat{\eta}_2, \dots, \hat{\eta}_{|\mathcal{Q}|}) > g(\eta_1, \eta_2, \dots, \eta_{|\mathcal{Q}|}) \geq \eta_{\text{vac}}$, where the equality holds due to (32), and the last inequality holds since φ satisfies (10). This contradicts the assumption that φ is an optimal solution. Therefore, there exists at least one equilibrium node in any hexagonal cell $k \in \mathcal{Q}$ in an optimal solution. This completes the proof. ■

REFERENCES

- [1] D. Ahn and S. Hong, "Effect of coupling between multiple transmitters or multiple receivers on wireless power transfer," *IEEE Trans. Ind. Electron.*, vol. 60, no. 7, pp. 2602–2613, Jul. 2013.
- [2] D. L. Applegate, R. E. Bixby, V. Chvatal, and W. J. Cook, *The Traveling Salesman Problem: A Computational Study*. Princeton, NJ, USA: Princeton Univ. Press, Jan. 2007, ch. 4.
- [3] E. M. L. Beale and J. J. H. Forrest, "Global optimization using special ordered sets," *Math. Program.*, vol. 10, no. 1, pp. 52–69, 1976.
- [4] Concorde TSP Solver [Online]. Available: <http://www.tsp.gatech.edu/concorde/>
- [5] C. A. Floudas, *Deterministic Global Optimization: Theory, Methods, and Applications*. Norwell, MA, USA: Kluwer, Dec. 1999, ch. 2.
- [6] K. Finkenzeller, *RFID Handbook: Fundamentals and Applications in Contactless Smart Cards and Identification*, 2nd ed. New York, NY, USA: Wiley, 2003, ch. 4.
- [7] S. R. Gandham, M. Dawande, R. Prakash, and S. Venkatesan, "Energy efficient schemes for wireless sensor networks with multiple mobile base stations," in *Proc. IEEE GLOBECOM*, San Francisco, CA, USA, Dec. 2003, pp. 377–381.
- [8] S. He, J. Chen, F. Jiang, D. K. Y. Yau, G. Xing, and Y. Sun, "Energy provisioning in wireless rechargeable sensor networks," in *Proc. IEEE INFOCOM*, Shanghai, China, Apr. 2011, pp. 2006–2014.
- [9] Y. T. Hou, Y. Shi, and H. D. Sherali, "Rate allocation and network lifetime problems for wireless sensor networks," *IEEE/ACM Trans. Netw.*, vol. 16, no. 2, pp. 321–334, Apr. 2008.
- [10] IBM, Armonk, NY, USA, "IBM ILOG CPLEX optimizer," [Online]. Available: <http://www-01.ibm.com/software/integration/optimization/cplex-optimizer/>

- [11] B. Jiang, J. R. Smith, M. Philipose, S. Roy, K. Sundara-Rajan, and A. V. Mamishev, "Energy scavenging for inductively coupled passive RFID systems," *IEEE Trans. Instrum. Meas.*, vol. 56, no. 1, pp. 118–125, Feb. 2007.
- [12] A. Kurs, A. Karalis, R. Moffatt, J. D. Joannopoulos, P. Fisher, and M. Soljacic, "Wireless power transfer via strongly coupled magnetic resonances," *Science*, vol. 317, no. 5834, pp. 83–86, Jul. 2007.
- [13] A. Kurs, R. Moffatt, and M. Soljacic, "Simultaneous mid-range power transfer to multiple devices," *Appl. Phys. Lett.*, vol. 96, pp. 044102-1–044102-3, Jan. 2010.
- [14] *Handbook of Batteries*, D. Linden and T. B. Reddy, Eds., 3rd ed. New York, NY, USA: McGraw-Hill, 2002, ch. 1.
- [15] J. Messina, "Haier exhibits a wireless HDTV video system at the 2010 CES," 2010 [Online]. Available: <http://phys.org/news182608923.html>
- [16] Y. Peng, Z. Li, G. Wang, W. Zhang, and D. Qiao, "Prolonging sensor network lifetime through wireless charging," in *Proc. IEEE RTSS*, San Diego, CA, USA, Nov. 30–Dec. 3 2010, pp. 129–139.
- [17] Powercast Corporation, Pittsburgh, PA, USA, "PowerCast," [Online]. Available: <http://www.powercastco.com>
- [18] A. K. RamRakhyani, S. Mirabbasi, and M. Chiao, "Design and optimization of resonance-based efficient wireless power delivery systems for biomedical implants," *IEEE Trans. Biomed. Circuits Syst.*, vol. 5, no. 1, pp. 48–63, Feb. 2011.
- [19] A. Sample, D. Yaniel, P. Powledge, A. Mamishev, and J. Smith, "Design of an RFID-based battery-free programmable sensing platform," *IEEE Trans. Instrum. Meas.*, vol. 57, no. 11, pp. 2608–2615, Nov. 2008.
- [20] Y. Shi and Y. T. Hou, "Some fundamental results on base station movement problem for wireless sensor networks," *IEEE/ACM Trans. Netw.*, vol. 20, no. 4, pp. 1054–1067, Aug. 2012.
- [21] H. D. Sherali, W. P. Adams, and P. J. Driscoll, "Exploiting special structures in constructing a hierarchy of relaxations for 0-1 mixed integer problems," *Oper. Res.*, vol. 46, no. 3, pp. 396–405, May–Jun. 1998.
- [22] H. D. Sherali and W. P. Adams, *A Reformulation- Linearization Technique for Solving Discrete and Continuous Nonconvex Problems*. Norwell, MA, USA: Kluwer, 1999, ch. 8.
- [23] B. Tong, Z. Li, G. Wang, and W. Zhang, "How wireless power charging technology affects sensor network deployment and routing," in *Proc. IEEE ICDCS*, Genoa, Italy, Jun. 2010, pp. 438–447.
- [24] G. Wang, W. Liu, M. Sivaprakasam, M. Humayun, and J. Weiland, "Power supply topologies for biphasic stimulation in inductively powered implants," in *Proc. IEEE ISCAS*, Kobe, Japan, May 23–26, 2005, pp. 2743–2746.
- [25] L. Xie, Y. Shi, Y. T. Hou, and H. D. Sherali, "Making sensor networks immortal: An energy-renewal approach with wireless power transfer," *IEEE/ACM Trans. Netw.*, vol. 20, no. 6, pp. 1748–1761, Dec. 2012.
- [26] L. Xie, Y. Shi, Y. T. Hou, and W. Lou, "Wireless power transfer and applications to sensor networks," *IEEE Wireless Commun.*, vol. 20, no. 4, pp. 140–145, Aug. 2013.

Yi Shi (S'02–M'08–SM'13) received the Ph.D. degree in computer engineering from Virginia Tech, Blacksburg, VA, USA, in 2007.



He is currently a Senior Research Scientist with Intelligent Automation, Inc., Rockville, MD, USA, and an Adjunct Assistant Professor with Virginia Tech. His research focuses on optimization and algorithm design for wireless networks.

Dr. Shi was a recipient of the IEEE INFOCOM 2008 Best Paper Award and the only Best Paper Award Runner-Up of IEEE INFOCOM 2011.

Y. Thomas Hou (S'91–M'98–SM'04–F'14) received the Ph.D. degree in electrical engineering from the Polytechnic School of Engineering of New York University, Brooklyn, NY, USA, in 1998.



He is a Professor with the Bradley Department of Electrical and Computer Engineering, Virginia Tech, Blacksburg, VA, USA. His research focuses on developing innovative solutions to complex problems that arise in wireless networks.

Prof. Hou was named an IEEE Fellow for contributions to modeling and optimization of wireless networks. He is on the editorial boards of a number of IEEE journals. He is the Chair of IEEE INFOCOM Steering Committee.

Wenjing Lou (S'01–M'03–SM'08) received the Ph.D. degree in electrical and computer engineering from the University of Florida, Gainesville, FL, USA, in 2003.



She is currently an Associate Professor with the Department of Computer Science, Virginia Tech, Blacksburg, VA, USA. Her research interests are cyber security and wireless networks.

Dr. Lou is on the editorial boards of a number of IEEE journals. She is the Steering Committee Chair of the IEEE Conference on Communications and

Network Security (CNS).

Hanif D. Sherali is a University Distinguished Professor Emeritus with the Grado Department of Industrial and Systems Engineering, Virginia Tech, Blacksburg, VA, USA. His research interests are analyzing problems and designing algorithms for specially structured linear, nonlinear, and integer programs arising in various applications, global optimization methods for nonconvex programming problems, location and transportation theory and applications, and economic and energy mathematical modeling and analysis.

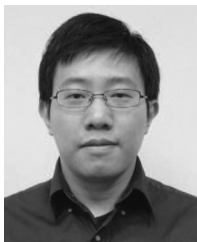


Prof. Sherali is an elected member of the US National Academy of Engineering (NAE).

Scott F. Midkiff (S'82–M'85–SM'92) received the Ph.D. degree in electrical engineering from Duke University, Durham, NC, USA, in 1985.



He is a Professor and Vice President for Information Technology and Chief Information Officer with Virginia Tech, Blacksburg, VA, USA. His research interests include wireless and ad hoc networks, network services for pervasive computing, and cyber-physical systems.



Liguang Xie (S'08–M'14) received the Ph.D. degree in computer engineering from Virginia Tech, Blacksburg, VA, USA, in 2013.

His research interests include optimization and algorithm design for wireless networks, with a current focus on wireless power transfer for energy-constrained wireless networks.